Géographie physique et Quaternaire

Talus fabric, clast morphology, and botanical Indicators of Slope Processes on the Chaos Crags (California Cascades), U.S.A.
Relevés botaniques, granulométrie, forme et organisation des débris sur les talus d'éboulis en tant qu'indicateurs des processus dans les Chaos Crags (monts Cascades, Californie, U.S.A.).
Morfología y orientación de derrubios clásticos, e indicadores botánicos de procesos de pendiente en Chaos Crags (Cascades, California)

Francisco L. Pérez

Citer cet article

Pérez, F. L. (1998). Talus fabric, clast morphology, and botanical Indicators of Slope Processes on the Chaos Crags (California Cascades), U.S.A. *Géographie physique et Quaternaire*, *52*(1), 47–68. https://doi.org/10.7202/004861ar

Résumé de l'article

Les Chaos Crags, un ensemble de dômes de dacite, ont subi des glissements de débris volcaniques vers 1675 ap. J.-C. qui ont laissé un volumineux dépôt et une cicatrice sur le flanc nord, maintenant recouverte de talus d'éboulis. On étudie ici les variations spatiales de l'organisation des éléments (fabrique), la morphologie des talus et les processus géomorphologiques présentement actifs. Le talus présente un profil en deux segments : le segment supérieur, plus raide, présente un profil rectiligne tandis que le segment inférieur est concave et plus court. Les débris sont granoclassés à la fois verticalement (les plus gros fragments vers le bas des talus) et horizontalement (les plus grosses particules sous les parois). Le classement selon la forme est moins défini, mais la sphéricité augmente et l'allongement diminue vers le bas. L'orientation des fragments dans le haut du talus (grands axes parallèles au plan et à la direction de la pente) montre que les fragments se sont déplacés par glissement, alors que les blocs de la base ont été déposés par éboulement, ce qui entraîne une orientation de type isotropique. Les observations de terrain et les données botaniques démontrent l'importance des glissements qui se produisent en raison de la présence d'une grande quantité de blocaille dans la partie supérieure. La comparaison avec d'autres versants semblables et la photographie répétée indique que le talus des Chaos Crags s'est formé rapidement après l'effondrement du dôme, alors que de nombreux débris se sont accumulés sous des murs rocheux instables. Le talus a connu une faible sédimentation au cours du XX ^{e} siècle et a été altéré par divers mouvements de masse, incluant les avalanches et les glissements de terrain.

TALUS FABRIC, CLAST MORPHOLOGY, AND BOTANICAL INDICATORS OF SLOPE PROCESSES ON THE CHAOS CRAGS (CALIFORNIA CASCADES), U.S.A.

Francisco L. PÉREZ, Department of Geography, University of Texas, Austin, Texas, 78712-1098, U.S.A., iago@mail.utexas.edu.

ABSTRACT The Chaos Crags, a group of dacite domes in the Cascades Mtns (California), were affected by volcanic debris avalanches *ca.* 1675 A.D.; these left a sizable deposit and a scar on the north mountain flank, now covered by talus. This report examines the fabric and morphology of talus debris, their spatial variation, and the geomorphic processes presently affecting the slope. The talus presents a bi-segmented profile with a steep upper rectilinear segment and a shorter concave, basal zone. Debris are sorted by size both along (larger clasts downslope) and across the talus (larger particles below the cliffs). Shape sorting is weaker, but clast sphericity increases, and elongation decreases, toward the footslope. Upper-talus fabrics (long axes parallel to talus plane and slope) show that clasts there move by sliding, while basal blocks are deposited by rockfall, which causes more isotropic fabrics. Field observations and botanical evidence indicate the overall significance of grain flows, which are prevalent due to an abundant supply of rubble on the upper talus. Comparison with similar recent slopes and repeat photography suggest the Chaos talus formed swiftly following dome collapse, when much debris may have collected below the unstable rockwalls. The talus has experienced only modest sedimentation during the 20th century, and is currently affected by 'normal' mass-wasting processes, which also include snow avalanches and debris flows.

RÉSUMÉ *Relevés botaniques, granulométrie, forme et organisation des débris sur les talus d'éboulis en tant qu'indicateurs des processus dans les Chaos Crags (monts Cascades, Californie, U.S.A.).* Les Chaos Crags, un ensemble de dômes de dacite, ont subi des glissements de débris volcaniques vers 1675 ap. J.-C. qui ont laissé un volumineux dépôt et une cicatrice sur le flanc nord, maintenant recouverte de talus d'éboulis. On étudie ici les variations spatiales de l'organisation des éléments (fabrique), la morphologie des talus et les processus géomorphologiques présentement actifs. Le talus présente un profil en deux segments : le segment supérieur, plus raide, présente un profil rectiligne tandis que le segment inférieur est concave et plus court. Les débris sont granoclassés à la fois verticalement (les plus gros fragments vers le bas des talus) et horizontalement (les plus grosses particules sous les parois). Le classement selon la forme est moins défini, mais la sphéricité augmente et l'allongement diminue vers le bas. L'orientation des fragments dans le haut du talus (grands axes parallèles au plan et à la direction de la pente) montre que les fragments se sont déplacés par glissement, alors que les blocs de la base ont été déposés par éboulement, ce qui entraîne une orientation de type isotropique. Les observations de terrain et les données botaniques démontrent l'importance des glissements qui se produisent en raison de la présence d'une grande quantité de blocaille dans la partie supérieure. La comparaison avec d'autres versants semblables et la photographie répétée indique que le talus des Chaos Crags s'est formé rapidement après l'effondrement du dôme, alors que de nombreux débris se sont accumulés sous des murs rocheux instables. Le talus a connu une faible sédimentation au cours du XXe siècle et a été altéré par divers mouvements de masse, incluant les avalanches et les glissements de terrain.

RESUMEN *Morfología y orientación de derrubios clásticos, e indicadores botánicos de procesos de pendiente en Chaos Crags (Cascades, California).* Los Chaos Crags, un grupo de domos de dacita en las Montañas Cascades (California), fueron afectados por varias avalanchas detríticas volcánicas *ca.* 1675 D.C; éstas dejaron un gran depósito de derrubios y una cicatriz en la ladera norte de la montaña, hoy día cubierta por talos. Se examina aquí la morfología y la orientación de las partículas del talo, la variación espacial de éstas, y los procesos geomorfológicos que actualmente afectan la pendiente. El talo muestra un perfil bi-segmentado con una porción superior rectilínea y empinada, y una zona cóncava basal más corta. Los derrubios están segregados por tamaño tanto a lo largo (clastos mayores en la base de la montaña) como al través de la pendiente (partículas mayores debajo de las paredes rocosas). Los fragmentos también están segregados por forma; su esfericidad incrementa hacia la base del talo, donde la elongación de las partículas es menor. La orientación clástica en el talo superior (ejes paralelos al plano y a la dirección de la pendiente) indica que las piedras se mueven allí por deslizamiento, mientras que los bloques al pie del flanco son depositados por caídas de rocas, que causan una orientación mas isotrópica. Las observaciones de campo y la evidencia botánica indican la importancia de los movimientos secos peliculares, asociados con un abundante suministro de derrubios en el alto talo. Comparación con otras pendientes recientes similares y foto-repetición sugieren que el talo en Chaos Crags se formó rápidamente tras el colapso del domo, cuando grandes cantidades de fragmentos deben haberse acumulado debajo de las inestables paredes rocosas. El talo ha experimentado sólo una modesta sedimentación durante el siglo 20, y hoy día es afectado por procesos geomorfológicos 'normales', que también incluyen aludes de nieve y flujos de barro.

INTRODUCTION

Catastrophic rockfalls (Porter and Orombelli, 1980) and associated deposits have received a great deal of attention in recent years. They are given different names, such as catastrophic rock- or land-slides, rock- or rockfall-avalanches, rockslide-avalanches, or sturzstroms (Crandell and Fahnestock, 1965; Shreve, 1966; Browning, 1973; Eisbacher, 1979; Butler *et al.*, 1986; Dawson *et al.*, 1986). These high-magnitude events are often triggered by earthquake activity. In addition, volcanic activity may cause similar large mass-wasting events, which are then more appropriately called volcanic debris avalanches (VDAs) (Siebert, 1984). Attention has focused on the causes of catastrophic rockfalls and on the deposits left by them. Many studies have described rock-fall deposits; in North America, recent or ancient debris deposits are found in several mountain ranges, including the Montana Rockies (Butler *et al.*, 1986), the Chugach Mountains of Alaska (Shreve, 1966) and the Mackenzie Mountains of northwestern Canada (Eisbacher, 1979). Sizable VDA deposits are common in the volcanic Cascade Range. Areas recently affected include Mount St. Helens (Voight *et al.*, 1983) and Little Tahoma Peak, Washington (Crandell and Fahnestock, 1965). Some studies, while focusing on the debris deposits, also contain cross-sectional views that include the source area, but none - to my knowledge - ever investigated the characteristics of the 'detachment scar', or of the talus slopes produced on the mountain flank by the catastrophic rockfall events, or their evolution with time.

The Chaos Crags is a group of dacite domes in the Cascades of northern California, where a series of VDAs *ca.* 1675 A.D. produced a large debris deposit (the 'Chaos Jumbles'), which covers nearly 8 km^2 and has a thickness of up to 40 m (Crandell *et al.*, 1974). The Chaos Jumbles have been studied by several researchers, starting with Howel Williams in 1928. Details about the geology of the Chaos Crags and Jumbles are given below, but it is pertinent to note that previous research has exclusively dealt with the Jumbles, and that little attention has been given to the talus cover on the scarred mountain flank below the collapsed dacite dome.

This study reports on the morphology of the talus aprons that have accumulated on the collapsed northern flank of the Chaos Crags since VDAs took place three centuries ago, and on the geomorphic processes that shape this talus at present. I will specifically examine the spatial variation of clast size, shape, and fabric, and of talus *texture* (*i. e.*, type of talus surface according to predominant particle size [Caine, 1967; Pérez, 1986]). I will then try to correlate these characteristics with the activity of different geomorphic processes. I have previously (Pérez, 1988a, b, 1989, 1990a) reported on the spatial trends of these parameters, and on the geomorphic agents which may influence them, on talus slopes on and near Lassen Peak. Those papers dealt with slopes that presumably have formed gradually by rockwall weathering during the Holocene. This study at Chaos Crags provides an unusual opportunity to generally contrast talus slopes of similar lithology, affected by comparable environ-mental parameters, but which have developed over widely different time periods. Site structure and topography clearly indicate that dome collapse and the VDAs removed any previous talus that might have covered the mountain flank (Williams, 1928, 1929, 1932). Three contrasting models of debris supply to the Chaos talus may be considered: (a) Some talus rubble - or perhaps even the bulk of it - may have been added by the VDAs; alternatively, (b) most of the slope debris were quickly deposited following the rockfall events; or (c) talus sediments have been deposited by gradual dome erosion during the last 300+ years. If talus debris were added by VDA events or soon afterwards, the slope may still display some significant differences from nearby 'normal' taluses gradually developed below dacite domes, but if the rubble was incrementally deposited post-collapse, few or no morphological differences might be evident.

Particle morphology and sorting are useful indicators of geomorphic processes acting on talus slopes. Many studies report increasing particle size downslope (Rapp, 1960a, b; Gardner, 1972; Bones, 1973; Albjär *et al.*, 1979; Pérez, 1986, 1988b, 1989). This occurs because: (1) large clasts gather momentum and bounce to the talus base; (2) this creates an upslope gradient of lower surface roughness; due to frictional resistance, other moving debris tend to stop near clasts of similar caliber, further reinforcing the sorting trend; (3) any small particles that reach the footslope fall in the openings between blocks ('sieve effect'; Carniel and Scheidegger, 1974).

Less often, a 'reversed' particle sorting (increasing clast size to the talus top) is found. This may eventually occur as debris supply from the rockwalls slowly decreases with time; the gradual reduction of rockwall height would allow most clasts to remain near the talus apex (Rapp, 1960a; Statham, 1973). Alluvial talus, where particles are transported by running water, also shows reversed sorting (Åkerman, 1984). Taluses affected by supranival aeolian transport develop reversed sorting as well (Hétu, 1995). Some talus slopes may exhibit no consistent downslope sorting (Griffiths, 1959; Caine, 1967). This can result from pronounced down-streaming of independent longitudinal debris 'tongues', which tends to produce, instead, a significant sorting across the slope (Brückl *et al.*, 1974; Pérez, 1986). Snow avalanche and debris-flow activity also yields poorly sorted deposits, as such processes may deliver large amounts of fine debris to the footslope (Gardner, 1972; Bones, 1973).

Particle shape variation is less frequently studied, probably because it usually shows a less clear trend than size. McSaveney (1971), Statham (1973), and Pérez (1986) found a gradual downward increase in clast sphericity, related to the greater ability of spherical particles to roll and bounce downhill. An abrupt increase in particle size and sphericity may occur on the basal talus, producing a distinctive 'basal fringe' of different particles (Rapp and Fairbridge, 1968). This may be caused by clast gliding over indurated snow, which allows larger and / or more spherical clasts to reach the base of the snow-covered talus (Pérez, 1989; Hétu, 1995). Even when present, shape sorting may be masked by the stronger size sorting (Statham, 1973).

Studies of particle orientation on talus have usually found that most long clast axes are aligned with the slope. Caine (1967) pioneered the study of three-dimensional talus *fabrics*; many reports have followed (McSaveney, 1971; Albjär *et al.*, 1979; Pérez, 1988a, b, 1989, 1990a; Hétu *et al.*, 1994, 1995; Hétu, 1995; Van Steijn *et al.*, 1995; Bertran *et al.*, 1997). These studies found that sliding clasts attain an alignment parallel or oblique to the slope and develop a slight uphill imbrication, while rockfall-deposited particles attain an isotropic fabric.

Talus studies often include slope profiles. A few have explored the internal structure of talus by means of seismic resonance techniques (Brückl *et al.*, 1974), but most simply describe the surface topography, focusing on general form, slope gradient, sharp discontinuities and perhaps debris and vegetation cover. Most talus profiles show an upper rectilinear segment and a sharply concave basal portion. This is often ascribed to an exponential (Poisson) distribution of distance of particle travel downslope (Kirkby and Statham, 1975). A more recent model of talus evolution (Francou and Manté, 1990; Francou, 1991) proposes that this topographic change occurs due to different slope processes; the upper talus functions both as deposit and transport surface, while the basal talus is affected exclusively by accumulation. A well-developed basal concavity may also occur from debris transport by snow and slush avalanches, or debris flows (Rapp, 1960a, b; Caine, 1969a). Infrequently, basal convex talus portions are found. These are the result of local debris supply that exceeds the ability of transport processes to distribute debris downslope (Albjär *et al.*, 1979); slope modification by large scale mass movements (Caine, 1969a); solifluction activity (Pérez, 1986); and presence of moraines (Pérez, 1989), protalus ramparts (Pérez, 1988a) or barriers - such as vegetation - which prevent debris from reaching the footslope (Hétu, 1989). Basal erosion by rivers or rock glaciers might also produce a convex talus profile.

PHYSICAL SETTING

Lassen Volcanic National Park (LVNP), is in northern California and has an area of 430 km^2 (Fig. 1). Lassen Peak (3193 m) marks the southernmost point of the volcanic Cascade range. The study area, the Chaos Crags (2592 m), is at 40° 32' N, 121° 30' W. The Lassen region is underlain by a complex series of basalt, andesite, and pyroclastic flows, interbedded with glacial deposits (Williams, 1932). Much of LVNP was affected by Holocene volcanic activity; Lassen Peak itself is a dacite dome extruded ~11,000 years BP in late Tioga time. The Chaos Crags were formed about 1200 years ago by extrusion of several dacite domes 5 km north of Lassen Peak (Crandell, 1972). Later, a dome on the NW side of the cluster collapsed, causing catastrophic rockfalls which travelled as far as 4.3 km from the mountain base and produced the Chaos Jumbles, a "chaotic assemblage of gigantic, loose, angular blocks" (Williams, 1928: 246). Two straight scar lines clearly mark the 1-km wide segment of the mountain flank which collapsed (Fig. 2). This scarred flank is presently occupied by massive talus deposits. A large depression lies below the talus; this is occupied by a small seasonal meltwater pond (Crags Lake). Williams (1928: 251) considered this depression to "...have been blasted through the loose debris...", and initially referred to it as a 'crater', but later (Williams, 1941) introduced the term 'explosion caldera' to refer to the hollow, thus emphasizing its unique volcanic origin (see Siebert, 1984: 165).

Different ages were initially proposed for the Chaos Jumbles. Williams (1928, 1929), based on the age of the oldest trees on the deposit, considered that this had formed 200 years prior to his visit (*i.e.*, ~1725 A.D.). Heath (1959, 1960) argued the Jumbles were actually composed of three different deposits, produced ~270, 750, and 1500 years BP, but was only able to confirm the age of the most recent event (~1690 A.D.) with tree-ring dating. His geologic evidence for the two older deposits was rejected by Crandell *et al.* (1974: 49), who concluded the Chaos Jumbles "...were formed by three or more high-speed air-cushioned avalanches, all of which occurred about 300 years ago." (*ca.* 1675 A.D.). Williams (1928) thought that such event(s) might have been triggered by volcanic or steam explosions, intrusion of another dome, or a strong earthquake. However, the tallest dome in Chaos Crags, directly south from the collapse area (Fig. 1), was emitting steam and gases between 1854 and 1857 (Williams, 1932); this supports the first two hypotheses. Following Siebert (1984: 178), who included the Chaos Crags in his comparative study of Quaternary VDAs, the event that produced the Jumbles is considered to have been a volcanic debris avalanche. A date between 1650 (Siebert, 1984) and 1675 (Crandell *et al.*, 1974) is accepted at present for the deposit.

Peaks in LVNP have enormous talus banks. Williams (1932: 203) noted that: "Scenically, the most striking feature of these mountains is the extraordinary development of talus on their flanks." Two factors account for this. The talus aprons girdling Lassen Peak, Chaos Crags and other domes originally resulted from the extrusion process, as domes rose through the debris produced by expansion and fracturing of their outer layers (Williams, 1932). The porphyritic hornblende-mica dacites also disintegrate easily, due to a high content of interstitial, intensely fractured glass (Williams, 1932; Pérez, 1988a). The original talus cover on the north flank of Chaos Crags was removed by the debris avalanches, and the present talus has been produced both by the collapse event itself, and by further debris accumulation during the past 320 years.

LVNP has a Mediterranean climate characterized by warm, dry summers, and cool winters with heavy snowfall. During summer, LVNP is under the influence of the North Pacific high, which blocks precipitation. In winter, as the high migrates south, storms move southeasterly into the region from the Aleutian low; thus, most precipitation falls between October and April (Crandell, 1972). Due to this strong seasonality, snowfall may represent 90 to 95 % of the annual total (Major, 1977). The closest station (Manzanita Lake, 1750 m [see Fig. 1]) shows a (1951-1980) mean annual precipitation of 1049 mm; ~91 % of this falls in the October - May period (Parker, 1992). Snow is redistributed by the prevailing westerlies, and sizable snow-fields accumulate on the
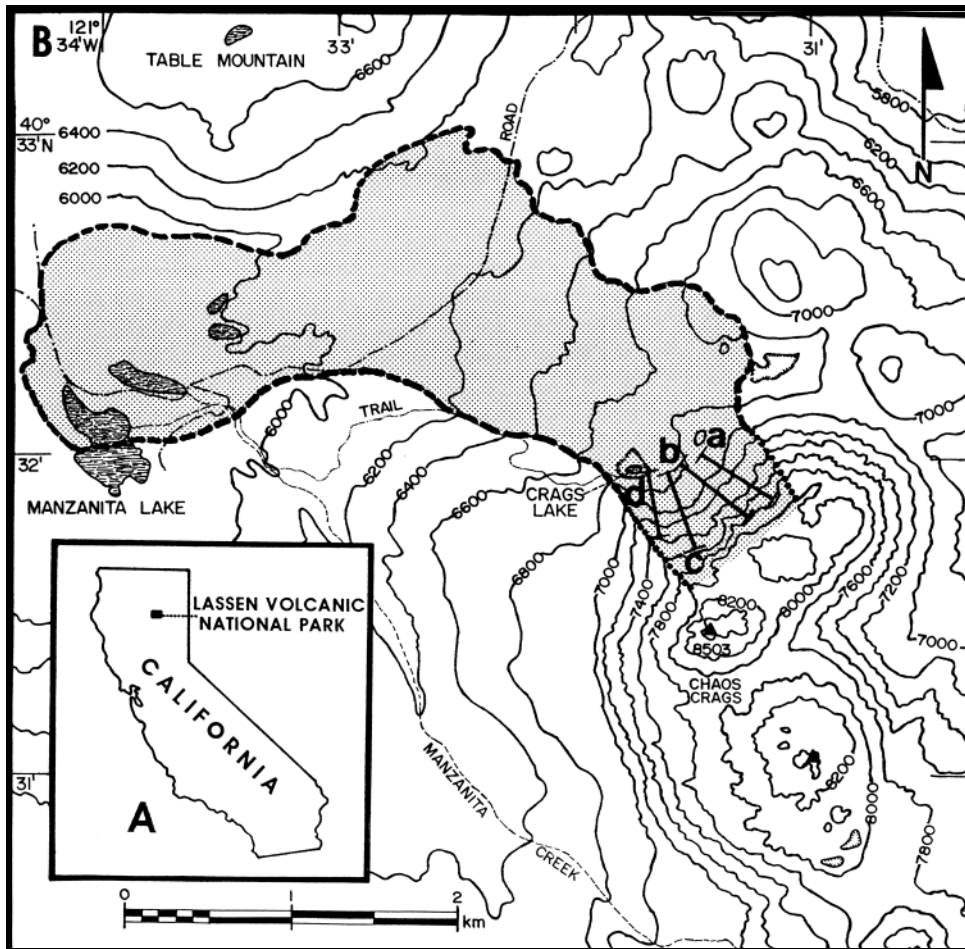
FIGURE 1. A: Location of Lassen Volcanic National Park in California. B. Location of study site. Shaded area shows approximate extent of the avalanche deposit (the 'Chaos Jumbles') and talus following collapse of the north dome of the Chaos Crags *ca.* 1675 A. D. The segment along the mountain flank that collapsed and is presently covered by talus deposits is located between the two dotted lines. Four lines (labelled a, b, c, d) indicate the position of the longitudinal talus profiles surveyed. Base map: Manzanita Lake (1956), U. S. Geological Survey, 15' quadrangle, 1: 62,500. Elevations in feet; contour interval is 200 feet. Graphic scale is in km.

A. Localisation du Lassen Volcanic National Park, en Californie. B. Localisation de la région à l'étude. La zone en grisé montre l'étendue approximative du dépôt d'avalanche (Chaos Jumbles) et du talus qui s'est formé à la suite de l'effondrement du dôme nord des Chaos Crags vers 1675 ap. J.-C. La partie située le long du flanc montagneux effondré, maintenant couvert par le talus d'éboulis, est situé entre les deux lignes pointillées. Quatres lignes (a,b,c,d) donnent l'emplacement des profils longitudinaux étudiés. Carte du Manzanita Lake (1956), U.S. Geological Survey, à 1/62 500. L'altitude est en pieds et les courbes de niveaux sont aux 200 pieds.

more sheltered (N, NE, E) slopes (Crandell, 1972). The snowpack is deep and persistent, and snow usually blankets most of the park from November to May. Snowpack depth at 2500 m commonly reaches 5 to 6.6 m in April /June, decreasing to ~3 m at 2180 m; large snow patches may persist through June above 2000 m (Taylor, 1995).

Mean daily temperatures remain below freezing in LVNP from November to April (Major, 1977). Average monthly temperatures at Manzanita Lake vary from -1.1 °C in January to 16.9 °C in July, but values below 0 °C are recorded at higher elevations in all months (Parker, 1992). Even in August, freezing occurs during 40 % of the nights at 2700 m (Pérez, 1988a). Thermal fluctuations are influential in rockfall occurrence, which reaches a peak in spring and early summer, when there is an ample supply of meltwater to most rockwalls (Rapp, 1960a; Gardner, 1970). Temperature oscillations during spring / early summer may also help produce a hard snow crust which facilitates descent of debris over talus (Ward, 1985; Pérez, 1988a, 1990a).

The *regional* forest line in LVNP is at ≥ 2440 m (Arno and Hammerly, 1984), but small tree islands of whitebak pine (*Pinus albicaulis*) or mountain hemlock (*Tsuga mertensiana*) may be found up to ~3060 m (Pérez, 1990b). Owing to the northerly aspect of the talus studied in this report, its *local*

undisturbed forest line is found at an elevation of only ~2130 m (Fig. 2). As the slope extends from about 2025 to 2400 m elevation, it lies right within the timberline zone.

Alpine soils have been scarcely studied in LVNP. Talus slopes on Lassen Peak have sandy-skeletal Lithic and Typic Cryorthents (US soil taxonomy: see Soil Survey Staff, 1994) with much gravel (≥ 60 %) and a sandy texture (Pérez, 1989). The bulk of the remaining finer fraction is silt; this suggests that frost weathering - perhaps aided by aeolian deposition - is the main agent of soil formation above timberline.

METHODS

FIELD TECHNIQUES

Four slope profiles were obtained from talus apex to base with compass, clinometer, and a tape stretched between stations at 10-m intervals. The two east transects (A, B) were mainly occupied by large clasts (cobbles, boulders), but the two west ones (C, D) had fewer clasts at the surface, which was covered by gravel or pebbles. The talus surface was sampled on stations every 50 m along the four profiles with a photographic technique (Caine, 1969b; Brückl *et al.*, 1974; Pérez, 1986). Transects A, B, and C had 8 sampling stations each, transect D only 5. At each station, a 100 x 70 cm grid was placed on the talus, and photos taken along a continu-

FIGURE 2. Northern flank of the Chaos Crags and the talus slopes below; west is to the right. The Chaos Crags summit (2592 m) is the conical peak on the upper right; elevation at the talus base is about 2000 m. The sectioned and partially collapsed dacite domes exposed during the volcanic explosion are at the center of the picture, above the talus. Two straight scars, produced by sliding of the mountain flank, are clearly visible at both sides of the photo. The scar on the left side shows as a transition line between the dark slope (the older talus near the edge of the photograph) and the lighter area (the recent talus) to the right of the scar line. The scar on the right side appears as a sharp ridge separating contrasting west-facing (older talus) and east-facing (new talus) slope areas. The area between the two scars is about 950 m wide. Note the position of the undisturbed forest line (at ~2130 m) on the right edge of the photograph. The foreground is occupied by the 'Chaos Jumbles', an extensive debris deposit now sparsely covered by invading conifers (the 'Dwarf Forest'). August 1991.

Flanc nord des Chaos Crags et les versants d'éboulis ; l'ouest est à droite. Le sommet des Chaos Crags (2592 m) est un pic conique à droite ; l'altitude à la base du talus est de 2000 m. Les dômes de dacite sectionnés et partiellement effondrés pendant l'éruptiom volcanique sont au centre, au-dessus du talus. Deux cicatrices rectilignes, causées par le glissement du flanc montagneux sont clairement visibles sur les deux côtés de la photographie. La cicatrice de gauche apparaît comme une ligne de transition entre le versant sombre (le plus vieux talus en bordure) et la partie plus claire (le talus récent) à droite de la ligne de cicatrice. La cicatrice de droite ressemble à une crête pointue séparant l'ancien talus exposé à l'ouest du nouveau talus exposé à l'est (950 m sépare les deux cicatrices). À noter à droite l'emplacement de la limite de la forêt (à ~2130 m), qui n'a pas été déplacée. Le premier plan est occupé par le Chaos Jumbles, un immense dépôt de débris, maintenant partiellement recouvert par des conifères (Dwarf Forest). Août 1991.

ous 10-m long, 70-cm wide, transect parallel to contours. These photo-transects were later sampled at 5-cm intervals (*i.e.*, 200 data points per transect) to calculate the percentage of the ground surface occupied by clasts or by fine debris - henceforth called *gravel* (particles < 5 cm along their longest or *a* axis). Particle-size data for transects C and D were determined by measuring the *a* axis of the 50 largest *clasts* (> 5 cm *a* axis) visible on the photo-transects (Pérez, 1989).

Clast morphology and fabric along profiles A and B were directly investigated in the field; data come from the same stations above. Fifty contiguous large surface clasts were measured on both sides of the transect, after a procedure by Ward (1985). Parameters determined include three axial lengths (*a*, *b*, *c* axes; Krumbein, 1941), number of clast faces (Caine, 1967), and *a* axis orientation and plunge (Goudie, 1981).

Detailed observations on activity of slope processes, the deposits left by them, and other evidence of process occurrence were gathered by extensive reconnaissance of the talus, flanks, and summits of the Chaos Crags during five consecutive summers (1989 - 1993). Plants are extensively used in this study as potential indicators of geomorphic activity. Presence and relative abundance of plant species was noted along transects. Specimens of all species found on the talus were collected and classified; taxonomic nomenclature follows Munz and Keck (1970). As part of a related study, the age of the largest 30 trees on the talus was determined by counting annual growth rings from cores extracted about 30 cm - the minimum height needed to turn the increment-borer - above the trunk base. In a few cases, dense low branches made it necessary to core the trees a bit higher. Fifteen specimens of western white (WW) pine (*Pinus monticola*) and 15 of ponderosa pine (*Pinus ponderosa*) were taken. The number of years needed for a seedling to reach coring height could not be determined, but based on calibration factors used by Heath (1959) for trees on the Chaos Jumbles and by Taylor (1990) for pines at similar elevations in LVNP, 7 yrs per 30 cm below coring height were added to ring-counted ages.

ANALYTICAL PROCEDURES

Regressions between proportional distance along the talus and slope angle were used to assess the degree of concavity along transects (*concavity index*, Gardner, 1972; Gardner *et al.*, 1983). Trends in debris size were studied with a *weighted average particle size* (WAPS) (Carniel and Scheidegger, 1974; Pérez, 1989), obtained by multiplying the percentage of the ground surface occupied by each texture (clasts or gravel) by their mean size, and adding these values. Clast volume was calculated on transects A and B, based on the three axial lengths; no correction factor was used for number of clast faces, as all blocks sampled had similar values (6 to 8 faces). Volume is expressed as a *nominal diameter* or 'diameter of an equivalent sphere' (Folk, 1980) in cm and in the phi (Ø) scale (Caine, 1967). The standard deviation in Ø units was used as a measure of *sorting* (Folk, 1980). Clast shape was mainly analyzed with three numerical indices: mean *sphericity* ($c^2/ [a \times b])^{.333}$, *elongation* (a / b), and *flatness* (a + b / 2c) (Goudie, 1981; Gardiner and Dackombe, 1983). Two additional indices, (c / a) and ([a - b] / [a - c]), were also calculated and used to project clast-shape distributions on ternary diagrams (Folk, 1980) (see Fig. 9). Data sets for all parameters were tested for normality. Most data sets were normally distributed, but some - notably those for flatness - were not, thus were transformed to $\log_{10}$; transformed data were accepted as normal (p < 0.05) (Jones, 1969).

Clast size and shape variation among and along transects was analyzed with one-way analysis of variance (ANOVA), but as this does not indicate *where* significant differences, if any, lie, multiple *t* tests were also used to con-

trast paired data sets. When several means are compared with *t* tests, the probability of obtaining a false significant difference between data sets is high (Thomas, 1973), and for a data set of eight means, this error probability is about 50 % (Steel and Torrie, 1960). Thus, *t* tests were validated with Duncan's Multiple Range (DMR) and with Scheffé's F tests (Duncan, 1955; Scheffé, 1953). The relationship between clast size and shape was examined with linear and logarithmic regressions for all parameters calculated for the 800 clasts sampled along profiles A and B. Regressions between the three clast axes were also run for 100 randomly selected clasts (Griffiths, 1959; Gardner, 1972; Pérez, 1986). Shape sorting along transects was examined with contoured ternary diagrams (Pérez, 1987) as well. The Kolmogorov-Smirnov (KS) test was used to compare percentages of clast shape classes along the transects (McSaveney, 1971). Details about clast fabric analysis are given below.

FIELD DATA RESULTS

SLOPE MORPHOMETRY

The transects were 250 to 530 m long, and covered an altitudinal span of 125 to 235 m. All were bounded at their apex by rockwalls, but these differed widely in size. The east transects (A, B), below the massive collapsed dome, had cliffs > 100 m tall (Fig. 3) while the west profiles (C, D) were below small isolated dome remnants only 18 to 25 m tall. Profiles A, B, and C merged gradually with debris-avalanche deposits at the talus foot, but D ended in a sizable depression > 120 m wide and 25 m deep partially filled by meltwater (Crags Lake, Fig. 1). Early in the season this lake - actually a pond - occupies most of the depression, but quickly shrinks during the hot summer days, and usually dries and disappears by late July or August.

Slope angle increased steadily upwards along the four sections, reaching a maximum value below the dacite walls; maximum gradient dropped gradually from transects A to D (Fig.4). All sections showed similar shapes: a predominantly rectilinear talus throughout most of the transect, and a well-developed concavity at the basal slope. Concavity indices were high, with similar correlation coefficients (r) for profiles A, B, and C, and highest along D (Table I). The first three transects showed a slightly abrupt break near the base, where angle dropped in a short distance from ≥ 20° to ≤ 7°. This break could not be discerned along section D, since its lower 15-25 m were covered by Crags Lake. This basal segment is also affected by lacustrine processes, such as wave activity, basal sapping, etc., around the receding margins of the pond, as attested by minute shoreline steps which gradually appear during the summer drought. The nearly total lack of vegetation on a horizontal belt directly above the pond also suggests that this depression remains filled with snow and / or water during most of the year.

THE VARIATION OF TALUS TEXTURE AND CLAST SIZE

Texture and clast size differed significantly among transects. There was a clear gradient of decreasing particle size from the east (transect A) to the west side (D) of the

FIGURE 3. Close-up view of sectioned dome remnant above the talus. The steep dacite rockwalls are nearly 200 m high at the center of the photograph; the view covers an area about 430 m wide. Note the rough surface of the brecciated, intensely fractured bedrock and the lack of any regular dome structure (*cf*. Williams, 1928: 245). Several old small debris-flow tracks can be seen issuing from couloirs on the lower right corner of the photograph (August 1991).

Gros plan des restes du dôme sectionné au-dessus du talus. Les murs rocheux escarpés font presque 200 m au centre ; la largeur atteint environ 430 m. À noter la surface raboteuse du substratum bréchique excessivement fracturé et l'absence de toute structure en véritable forme de dôme (voir Williams, 1928: 245). Au coin inférieur droit, on peut voir plusieurs anciennes traces d'écoulement de petits débris issues de couloirs (août, 1991).

talus (Table II). One-way ANOVA and *t* tests indicated that the two east transects below the tall cliffs and with a substantial cover of blocks (Fig. 5) formed a discrete ['coarse'] set. The two west profiles, where clasts were smaller and most of the surface was occupied by gravel and pebbles (Fig. 6) formed another distinctive ['fine'] group. Clast size, degree of gravel cover, and WAPS differed significantly between these two transect groups (p < 0.001)..

TABLE I

General slope characteristics along the four talus transects investigated. Rockwall height above transects A and B was estimated from photographs and topographic maps (See Fig. 1 for transect location)

Transect	Aspect	Length (m)	Maximum Inclination	Concavity Index(*)	Rockwall Height (m)
A	262°	490	37.5°	0.939	~120
B	285°	500	37.4°	0.936	~145
C	313°	530	36.8°	0.937	20 - 25
D	320°	250	35.3°	0.974	18 - 20

(*): Correlation coefficients (r) of regressions between log-transformed distance along the talus and slope angle; all regressions significant at p < 0.001 level.

In addition to these contrasts among profiles, clast size and talus texture showed pronounced variation within transects: size of clasts and the percentage of the slope surface they occupied (thus also the WAPS) increased toward the basal talus. Gravel cover was always much higher near

FIGURE 4. Longitudinal profiles of the talus. Slope angle values shown are averages of 5 measurements taken at transect stations, and correspond to 50-meter long sections. All graphs are oriented from SE-SSE (left) to NW-NNW (right); see Fig. 1 for transect location. Transect D shows the level of Crags Lake at the time of profile survey (Aug. 16, 1991). Blank labelled arrowheads indicate location of sampling stations for particle morphology and texture. Shaded outlines show approximate extent of the dacite outcrops above the talus. Elevations along the left margin of sections are in meters; drawings do not show any vertical exaggeration.

Profils longitudinaux des talus. Les inclinaisons sont des moyennes de cinq mesures prises à des emplacements le long des transects qui correspondent à des segments de 50 m de long. Tous les graphiques sont orientés du SE-SSE (à gauche) vers le NO-NNO (à droite) ; la figure 1 donne la localisation des transects. Le transect D illustre le niveau du Crags Lake au moment du levé (16.08.91). Les triangles donnent la localisation les lieux d'échantillonnage. Les parties ombrées montrent la hauteur approximative des affleurements de dacite au-dessus du talus. Les altitudes sont en mètres il n'y a pas d'exagération verticale.
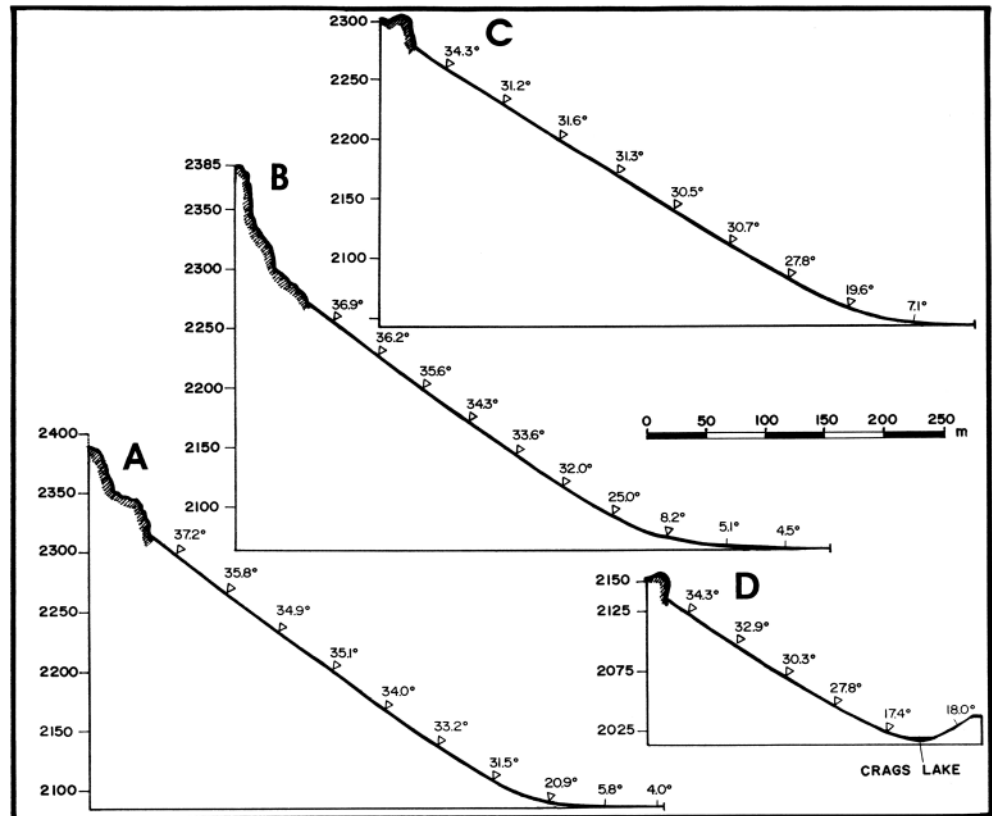

FIGURE 5. East side of the Chaos talus, near transect A. Note the large blocks covering the talus nearly to its apex; light zones below cliffs are occupied by finer debris. The dark circular patches on boulders are prostrate shrubs of rock spirea (*Holodiscus microphyllus*). Shrubs have diameters ranging from ~1.3 to 2.8 m (large, darker shrub on lower talus). July 1991.

*Versant est du talus du Chaos, près du transect A. À noter les gros blocs qui jonchent le talus près de son point le plus élevé ; des débris plus fins recouvrent les parties claires sous l'escarpement. Les taches sombres circulaires sur les blocs sont des formes prostrées d'arbrisseaux (*Holodiscus microphyllus*) dont les diamètres varient entre ~1,3 et 2,8 m (à la partie inférieure du talus). Juillet 1991.*
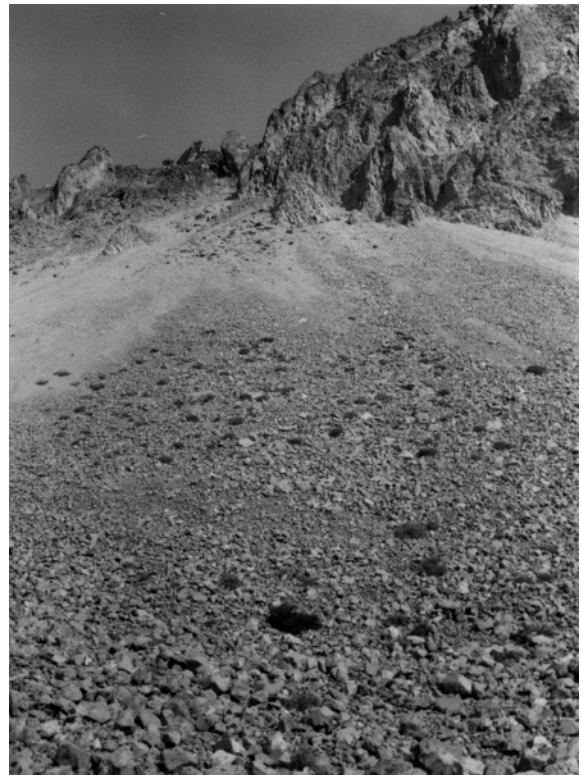
TABLE II

Clast size and surface texture variation along talus transects. Sampling transects start at the basal talus. Clast size data give averages of the a axis length of 50 particles on each sampling plot. Data for transects A and B were measured directly in the field; data for transects C and D were obtained from photo-transects. Sorting index is the S.D. of clast size in Ø units. The percentage of gravel indicates the fraction of the slope surface occupied by a fine (gravel) texture. The WAPS (weighted average particle size) combines the variation of both clast size and talus texture (see text for further detail).

Plot No.	Transect A				Transect B				Transect C				Transect D			
	Clast size (cm, Ø)	Sorting index	% of gravel	WAPS (cm)	Clast size (cm, Ø)	Sorting index	% of gravel	WAPS (cm)	Clast size (cm, Ø)	Sorting index	% of gravel	WAPS (cm)	Clast size (cm, Ø)	Sorting index	% of gravel	WAPS (cm)
1	56.4, -9.09	.377	0.5	56.1	40.2, -8.58	.457	0	40.2	42.6, -8.69	.38	0.5	42.4	21.5, -7.68	.433	35.5	14.8
2	46.8, -8.82	.391	0	46.8	40.8, -8.62	.403	1	40.4	23.2, -7.8	.386	7	21.7	13.4, -7.0	.425	67.5	6.0
3	43.1, -8.72	.321	0	43.1	27.2, -8.05	.332	0	27.2	14.4, -7.15	.245	5	13.8	12.9, -6.97	.372	63.5	6.3
4	33.9, -8.37	.312	1.5	33.5	25.4, -7.94	.376	0.5	25.3	8.2, -6.32	.346	73.5	4.0	14.4, -7.08	.519	68	6.3
5	34.0, -8.38	.289	29.5	24.7	27.9, -8.07	.393	0	27.9	7.4, -6.12	.51	86	3.2	7.5, -6.15	.451	85.5	3.2
6	35.7, -8.45	.28	4.5	34.2	32.2, -8.29	.339	0	32.2	8.7, -6.4	.329	69.5	4.4	-	-	-	-
7	26.6, -8.02	.317	47.5	15.1	32.2. -8.27	.391	0.5	32.0	7.0, -6.07	.442	96	2.7	-	-	-	-
8	25.3, -7.95	.283	49	14.1	38.8, -8.51	.499	12	34.4	9.5, -5.64	.498	85	3.6	-	-	-	-

the talus apex than at the footslope, but gravel increment along transects was not gradual. Tests showed that a sharp rise in gravel cover produced two significantly different (p < 0.001) sets of plots [plot N is in brackets] along transects B ([1-7] vs [8]), C ([1-3] vs [4-8]), and D ([1] vs [2-5]) (Table II). Gravel rise upslope transect A was similar but spottier; a main texture break was detected above plot 4, and another one below plot 7 (see Table II).

Axial clast length showed a complex variance. Maximum mean clast size and WAPS were found on basal plots - except on B, but the drop in *a*-axis length was more abrupt along transects such as C, where size range was greatest (Fig. 7). Clast size dropped steadily toward the talus apex along all transects except B, where the lower-middle slope had the smallest particles; a 'reversed' sorting was found above this area (Table III). DMR, F, and *t* tests show that on all profiles clast size variance results in homogeneous groups of basal-talus plots (one plot for A, C, and D; two plots for B) which are significantly different (all at p < 0.001) from those found immediately above them. Tests suggest the presence of three or four such discrete groups along each transect, which show no overlap except on transect B, where upper-talus plots are *not* statistically different from those at the foot-slope (Fig. 7). The results show that, for the chosen sampling interval (50 m), changes in clast size occur swiftly along the talus; however, a shorter interval might perhaps reveal more gradual changes.

Clasts were 'very well to well sorted' (Folk, 1980) on all sampling plots, as their sorting index (Ø S.D.) was between ~0.28 and 0.5 Ø (Fig. 8). Degree of clast sorting on plots showed no clear trends along slopes, but slightly greater indices (*i.e.*, *less* pronounced sorting) were seen both on basal-talus and talus-apex plots. This simply means that primarily large particles (on the former), or small (on the latter), lie next to distinctly smaller or larger debris, respectively.

THE VARIATION OF CLAST SHAPE

Clast shape variation along transects A and B was more gradual, and showed a less clear spatial pattern, than that observed for size. On both profiles, sphericity increased toward the slope base, elongation and flatness toward its apex (all ANOVAs are significant at p < 0.001) (Table III).
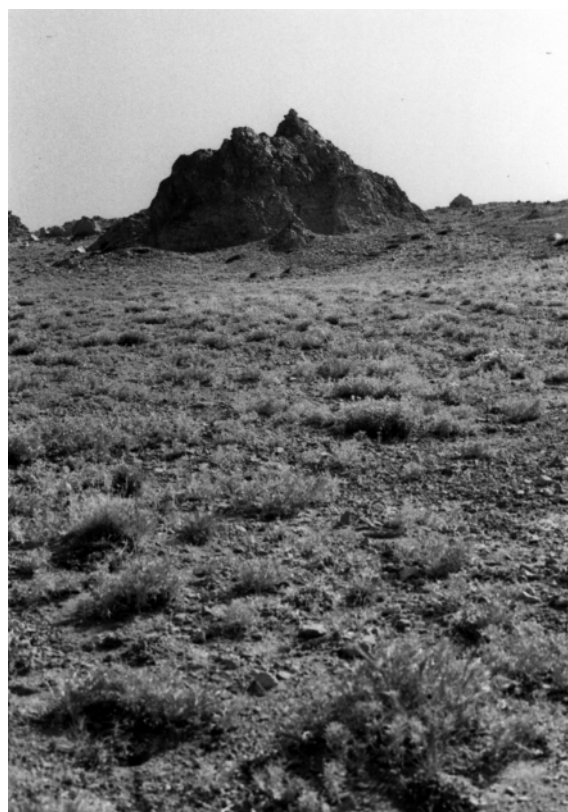

FIGURE 6. West side of the Chaos talus, near transect C. Note the smaller particle size (*cf.* Fig. 5) and denser vegetation cover, mainly of silverleaf lupine (*Lupinus obtusilobus*), coyote mint (*Monardella odoratissima*) and phacelia (*Phacelia frigida*). A small conical dacite outcrop appears at the talus apex. August 1991.

Versant oues du talus du Chaos, près du transect C. À noter la granulométrie plus fine (voir fig. 5) et le couvert végétal plus dense, surtout composé de Lupinus obtusilobus, *de* Monardella odoratissima *et de* Phacelia frigida. *Un petit affleurement conique de dacite coiffe la partie supérieure du talus (août 1991).*
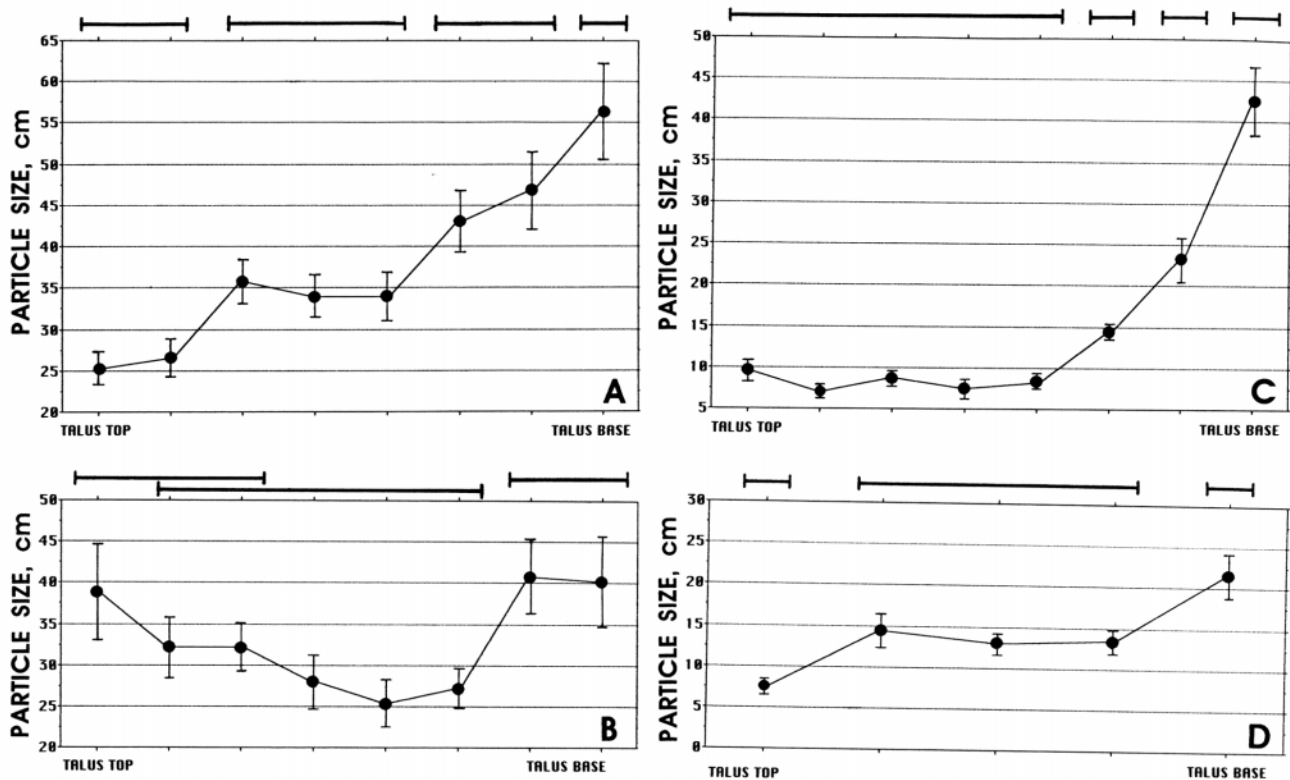
FIGURE 7.   Average clast size (long axis) along talus transects. Talus apex is on the left side of diagrams. Vertical bars indicate statistical confidence intervals (p < 0.001) for a *t* distribution. Whenever the bars for any two plots overlap, their mean clast size is not significantly different. Dark horizontal bars above the diagrams show homogeneous groups of statistically similar plots (p < 0.001), as identified by Duncan's Multiple Range test. See text for further details.

Taille moyenne des fragments (grand axe) le long des transects. Le sommet des talus est à gauche. Les barres verticales donnent l'intervalle de confiance (p < 0.001) pour une distribution t . Lorsque les barres coïncident, la dimension des fragments n'est pas significativement différente. Les barres horizontales au-dessus des diagrammes montrent des ensembles homogènes de relevés statistiquement semblables (p < 0,001), selon le test de Duncan (voir les détails dans le texte).

Flatness ratios showed a high inverse correlation ($r^2 = 0.944$ on A, 0.95 on B; both at p < 0.001) with sphericity indices (Goudie, 1981). All tests indicated that clast shape changes were somewhat more pronounced either at the talus top or its base, but overall shape variance was gradual. DMR and F tests identified several discrete plot groups (two to five, depending on transect or shape parameter) with statistically similar plots (p < 0.001), but which partially overlapped with other such groupings along the slope. In other words, important changes in clast shape *do* take place along both transects, and the upper- and lower-most plots there differ significantly from each other (p < 0.001) (Table III) but, in contrast to size variance, shape changes occur incrementally, thus no distinct zones or sharp breaks are detected on the talus.

Clast shape data were combined in four sets of two plots each according to relative slope position - upper (U), upper middle (UM), lower middle (LM), lower (L) (Pérez, 1989) - and plotted on ternary diagrams to assess the progressive sorting of fragments visually by shape (Fig. 9). The diagrams, each based on 100 clasts, show that these become gradually more compact (clustered on the upper corner of

the triangle) downslope; this seems a bit more pronounced along transect B. KS tests comparing the percentage of all *compact* clasts (C, CP, CB, and CE in Fig. 9) (McSaveney, 1971) verified this, as well as the subtle nature of shape variance. On transect B, clasts on the L and LM slopes are similar, and significantly more compact (p < 0.001) than those on the UM and U slope, which form another distinct group. Along transect A, particles on the L, LM, and UM slopes are comparably equidimensional, but all differ (p < 0.025) from the clasts on the U slope, which are significantly less compact. These data suggest that larger clasts may be somewhat more spherical than smaller fragments.

Regressions also indicated that, as clasts increase in size downslope, they also become less elongated and flattened, and attain a greater sphericity, but these relations between size and shape were not strong. Correlation coefficients (r) between nominal clast diameter and shape parameters were low, but all were higher along section A (flatness: -0.344, sphericity: 0.321, elongation: -0.237; all significant at p < 0.001) than along B (flatness: -0.123, sphericity:0.118, elongation: -0.107; significant at p < 0.05). The greater association of size and shape on the first profile seems related to

TABLE III

Clast morphology along transects A and B. Sampling transects start at the basal talus. Data indicate averages of 50 measurements at each sampling plot

Plot	Nominal Diameter (cm, Ø)	Sorting (Ø S.D.)	Elongation Index (*)	Sphericity Index (*)	Flatness Ratio (*)
Transect A:					
1	45.3, -8.77	0.393	1.454	0.733	1.661
2	35.9, -8.44	0.382	1.541	0.709	1.782
3	34.3, -8.38	0.349	1.482	0.728	1.666
4	25.3, -7.96	0.29	1.533	0.675	1.919
5	26.6, -8.02	0.33	1.512	0.717	1.721
6	27.5, -8.07	0.321	1.529	0.704	1.785
7	19.3, -7.57	0.275	1.598	0.672	1.914
8	18.1, -7.47	0.28	1.595	0.649	2.105
Transect B:					
1	32.2, -8.26	0.441	1.420	0.714	1.768
2	33.4, -8.32	0.433	1.399	0.730	1.715
3	22.5, -7.78	0.307	1.411	0.759	1.568
4	20.4, -7.62	0.368	1.418	0.719	1.735
5	21.3, -7.68	0.383	1.491	0.678	1.921
6	24.2, -7.88	0.347	1.565	0.693	1.852
7	24.0, -7.84	0.427	1.538	0.657	1.976
8	26.6, -7.98	0.45	1.617	0.609	2.368

(*): One-way ANOVA, Duncan's Multiple Range and Scheffe's F test indicate significant differences (p < 0.001) exist on both transects between the lowermost and uppermost plots. See text for further details.
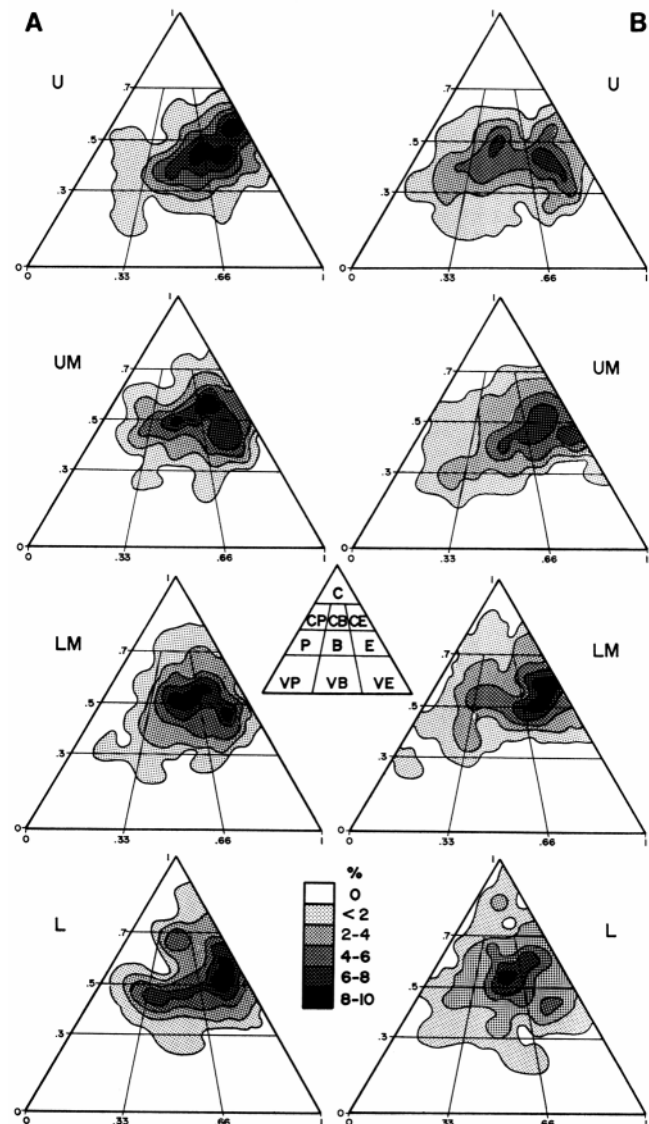

FIGURE 9. Contoured clast-shape diagrams (after Folk, 1980; Pérez, 1987) for four relative slope positions along transects A and B. Each diagram is based on 100 clasts (two sampling plots combined). Key for slope position: U = upper, UM = upper middle, LM = lower middle, L = Lower. Clast density is indicated by shades. Shape classes: C = compact, CP = compact platy, CB = compact bladed, CE = compact elongate, P = platy, B = bladed, E = elongate, VP = very platy, VB = very bladed, VE = very elongate.

Diagrammes triangulaires de la forme des fragments (selon Folk, 1980 ; Pérez, 1987) à quatre emplacements le long des transects A et B. Chacun des diagrammes s'appuie sur 100 fragments (combinaison de deux relevés). Emplacements : U = supérieur, UM = moyen supérieur, LM = moyen inférieur, L = inférieur. La densité des fragments est donnée par la trame. Classes de formes : C = compact, CP = compact plat, CB = compact en lame, CE = compact allongé, P = plat, B = en lame, E = allongé, VP = très plat, VB = en lame prononcée, VE = très allongé.

FIGURE 8. View of the upper middle talus in an area covered by well-sorted, 8 to 12 cm-long blocks and cobbles. Scale is in dm (long shaded bars) and in cm. August 1991.

Vue du talus dans sa partie moyenne supérieure recouverte par des blocs et des galets de 8 à 12 cm de long bien triés (échelle en dm et cm). Août 1991.

the continuous rise in clast size down the talus (Fig. 7A), while the more erratic size variation found on transect B (Fig. 7B) probably resulted in a weaker correlation. Regressions between the axes of 100 clasts (Gardner, 1972; Pérez, 1986) also indicated similar relationships between particle size and shape attributes, but were much less discriminating than the tests above to indicate any relevant spatial associations.

CLAST FABRIC

Particle fabric data were also combined in four sets of two plots each, which correspond to the relative slope positions (U, UM, LM, L) above. As fabric diagrams and statistics are based on data sets of 100 clasts, they are likely to show more clearly defined orientations than those for the eight individual sample plots - which contain only 50 points each - (Stauffer, 1966). Fabric trends were similar along the two sections (Fig. 10). Fabrics on the upper talus half (U+UM) have a well-defined subhorizontal girdle which coincides with the local slope; the principal mode, with *a* axis densities of 6-10 %, is superimposed on this girdle and parallel to the slope direction. Many clasts dip downtalus and plunge slightly less than the slope plane, thus exhibit an upslope imbrication. Overall, these fabrics show that most particles lie on the high talus with their long axes roughly parallel to the talus surface and slope line. Some noticeable fabric changes occur on the lower talus. The slope girdle becomes less continuous and pronounced, and main axial modes switch to an oblique position on the LM zone. This is even more pronounced on the L segment of A, where the main modes are nearly perpendicular to the slope; in addition, many particle axes are randomly scattered throughout the diagram, pointing in all directions. On the basal B talus, a dense main mode has migrated to the diagram center, indicating that the bulk of the clasts plunge steeply into the slope plane.

Fabrics were analyzed following a sequence of statistical procedures described in detail by Steinmetz (1962); this vectorial method allows a *three-dimensional* analysis of clast attitude, as data for both the azimuthal orientation and the dip of the *a* axes are combined. In addition, clast alignment was studied with the Vector Magnitude (L %) (Curray, 1956), a *two-dimensional* method restricted to azimuthal data which provides some measure of the strength of preferred particle orientation. It must be noted that this procedure does not analyze true clast *fabrics*, and it is therefore more appropriate for the analysis of basically 'planar' features such as soil- or sorted stone-stripes (Hall, 1979; Pérez, 1984, 1992) with an inclination concordant to that of the substrate. However, due to its simplicity, the method has been widely used. Consequently, the results of this report can be easily compared with those of other studies (Bertran *et al.*, 1997).

Following Steinmetz (1962), resultant vectors were obtained by rotation of axial orientations to the (0°-180°) hemisphere; thus, data show *angular differences* between the mean vector and (down)slope direction. Resultant vector directions become progressively more oblique on both profiles toward the basal talus, where vector dip also attains a greater angular difference with the talus plane (Table IV). The *imbrication index* (percentage of clast axes that plunge
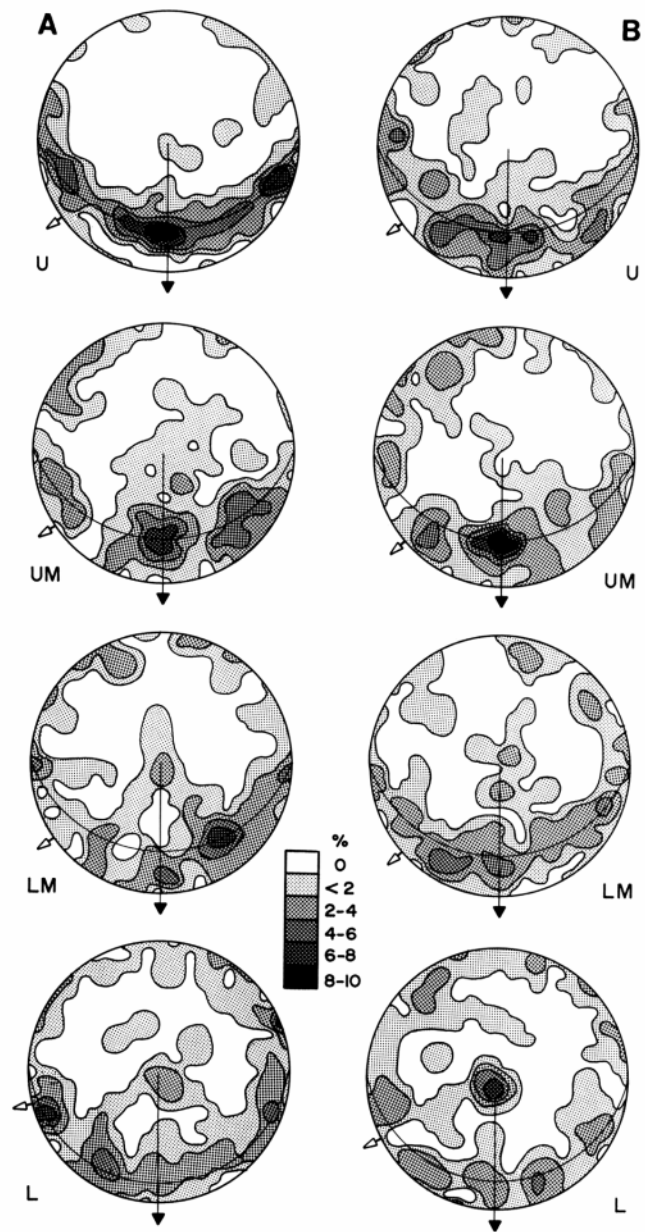

FIGURE 10. Clast fabric for relative slope positions along transects A and B. Each diagram is based on 100 clasts (two sampling plots combined). Key for slope position as in Figure 9. Contoured Schmidt stereonets were projected on the lower hemisphere; shades indicate the density of projections of the long particle axes (see graphic scale). The intercept of the slope plane is shown by the great circles. Slope direction (indicated by a dark arrowhead) is towards bottom of page; true north is shown by an empty arrowhead

Orientation des fragments selon l'emplacement relatif le long des transects A et B. Chacun des diagrammes s'appuie sur 100 fragments (combinaison de deux relevés). Voir la légende de l'emplacement à la figure 9. Stéréogrammes de Schmidt (hémisphère inférieure) sur lesquels les trames reflètent la densité des projections des grands axes des particules. Le grand arc de cercle représente l'inclinaison du versant. La direction de la pente (vers le bas) est donnée par la flèche tramée ; la flèche non tramée indique le nord géographique.

less than the slope plane) (Albjär *et al.*, 1979) also drops steadily down talus. KS tests showed that within-transect imbrication differences are significant (p < 0.001) only between the U and the L populations, but detected no between-transect differences when plots at the same relative slope position were compared. A test for randomness of orientation (Watson, 1956) showed all clast populations were significantly oriented (p < 0.01); however, greater vector strength values (*R*) (Steinmetz, 1962) on transect A indicate that particles there are more sharply oriented than on B (Table IV). In both transects, R is highest on U plots, and gradually drops toward the footslope. A regression of *R* and the vector's angle with slope direction (Pérez, 1989) gave a significant (p < 0.025) $r^2 = 0.799$, indicating that, in all data sets, fabrics more closely aligned with slope direction (*i.e.*, near the talus apex) *also* have a denser clustering of clast axes about their mean vectors. This is validated by an ANOVA of diameter values (2O) of the basal circle for a *cone of statistical confidence* (Fisher, 1953) (p < 0.001) centered about the resultant vector. On both profiles, 2O is lowest on the U area, and steadily increases toward the basal talus (Table IV).

K, a 'precision parameter' (Fisher, 1953) allows vector strength comparisons; low *K* values result with a high dispersion of axes about the mean vector. *K* values were tested with the maximum F-ratio for heterogeneity of variance (Hartley, 1950; tables in David, 1952). This test showed that U plots of both transects are significantly different (p < 0.01) from all the other plots on the same transect. The larger F on B (1.679) indicates fabric differences along this transect are somewhat stronger than along A (F= 1.478). In essence, *all* these statistical procedures confirm the pronounced fabric contrasts, graphically shown on Figure 10, between upper and lower talus zones.

Following Curray (1956), no distinction was made between opposite ends of the particles; analysis of L % values was made only in a range of 180° after axial rotation to one hemisphere. Vector magnitude was computed after doubling the angles of azimuthal data (Doornkamp and King, 1971: 346); this is needed in order to obtain a non-symmetric periodic distribution which reflects the true central tendency of data sets (Krumbein, 1939; Curray, 1956).

Vector magnitude showed gradually increasing values upslope on both transects (Table IV). Maximum L values (~45 %) were similar along both profiles; the downslope drop in L % was more pronounced on B, where the lowest L (19.5 %) was found. Comparable spatial trends were recently reported (Bertran *et al.*, 1997: table 1) along talus slopes in SW France. Vector magnitudes were analyzed with the Rayleigh test (Curray, 1956: fig. 4); this indicated that all data sets, except the lowest plot on transect B, were significantly oriented (p < 0.001). The L % data confirm the findings of the three-dimensional vectorial analyses: clast orientations along both transects become increasingly stronger as the talus apex is approached.

FIELD OBSERVATIONS OF PROCESS ACTIVITY

The talus at Chaos Crags is presently affected by different processes. Observations of specific geomorphic events, and of deposits and other kinds of evidence of their activity, indicate that rockfall activity, dry debris slides, snow-related processes (including snow avalanches), and debris- and mud-flows are the most significant agents of debris transport on the Chaos Crags.

TABLE IV

Clast fabric statistics according to relative slope position. Each slope position includes data from two consecutive sampling plots (= total of 100 particles). Sampling transects start at the basal talus.

Slope Position	Angular Difference (1)	Resultant Vector Dip	Angular Difference (2)	Imbrication Index (%)	Vector Strength (R)	Diameter, Cone of Confidence (*)	K (Precision Parameter)	L % (Vector Magnitude)
Transect A:								
L	62.3°	30.3°	+11.3°	22	73.28	26.4°	3.71	32.33 [a]
LM	61.8°	28.8°	-3.4°	38	72.31	27.0°	3.58	35.42 [a]
UM	52.9°	35.0°	+1.8°	41	73.38	26.3°	3.72	36.19 [a]
U	50.3°	27.3°	-6.2°	51	81.27	20.9°	5.29	45.43 [a]
Transect B:								
L	76.8°	34.9°	+12.6°	29	64.22	32.6°	2.77	19.46 [b]
LM	59.8°	34.1°	+2.3°	42	71.0	27.9°	3.41	27.32 [a]
UM	55.1°	33.8°	+0.4°	40	68.09	29.9°	3.1	37.34 [a]
U	49.2°	28.8°	-5.3°	56	78.71	22.7°	4.65	44.7 [a]

(*) : All values are significant at p < 0.001 level. Rayleigh test for L %: ([a]): p < 0.001; ([b]): p < 0.05.
Key for slope positions: L = Lower; LM = Lower Middle, UM = Upper Middle, U = Upper.
All data refer to Steinmetz (1962) vectorial analysis, except L %, which is the 'vector magnitude' of Curray (1956). Key: Angular difference (1): [Slope direction] minus [resultant vector azimuth]. Angular difference (2): [Slope inclination] minus [resultant vector dip]. Superscript letters refer to the significance levels of a Rayleigh test for L % values.

ROCKFALL ACTIVITY

The general aspect of the study site, coupled with its intensely fractured bedrock, provides an ideal setting for rockfall activity, especially during summer. A northern exposure allows much snow to persist on the Chaos Crags well into the warm season; this provides an ample supply of moisture to the rockwalls. In addition, the north face experiences broad daily temperature fluctuations, which greatly affect rockfall occurrence (Gardner, 1983).

Examination along the cliff bases showed highly fractured, brecciated dacite, with no lichen or vascular plant cover. Sizable fresh-looking, lighter-colored patches, presumed to be areas of recent rockfall activity, were evident on the rockwall face, notably above transect B. Some small impact craters and aligned bump holes (Rapp, 1960b) on the upper talus also indicated areas of recent rockfall. Actual rockfall events were witnessed on numerous occasions. However - and despite some initial apprehension about spending much time below the 'unstable' cliffs of the Crags - rockfall events were not very spectacular. Most rockfalls were small, removing only a few cubic meters of material; many events took place directly above couloir areas incised along the base of rockwalls (Fig. 3). Nearby events were easily noticed by the noise of falling debris; distant events were often evident by sizable dust clouds caused by falls (Clark *et al.*, 1972) or by large bouncing blocks that continued down the talus. Rockfalls had a tendency to cluster about mid-day hours; most events observed took place between noon and 3 p.m., when rock- wall temperatures peak in their diurnal cycle (*cf.* Gardner, 1983). Rockfalls were often tightly time-clustered, several events occurring within minutes in the same cliff area, even under clear skies. This may happen because, following an initial rockfall, the change in stability on the cliff face provides a greater chance for other rockfalls to occur (Luckman, 1976).

Most rockfall debris were transported only a short distance and remained on the U or UM talus after rolling and sliding on its surface; however, large boulders normally separated from moving debris masses and continued to the footslope. On one such event, a block ~110 cm long (later located) detached from the falling mass and quickly bounced downhill > 450 m to the basal talus. Some rockfalls must occur on snow-covered talus; this may affect the distance of debris travel. As noted above, a hard snow crust allows debris descent to the footslope, but soft snow (*i.e.*, in winter) could mire even large blocks, which may remain on the high talus following snow melt. Such an event seems to have taken place during the 1990-91 season, when a sizable rockfall produced a fresh scar area 6-10 m^2 on the cliff above transect C; many massive blocks and much fine debris from the event were left on the upper talus, 20-30 m below the rockwall base.

Many rolling and bouncing blocks must reach the footslope; ample evidence for rockfall impact is found in talus vegetation. Forty plant species (5 trees, 6 shrubs, 25 herbs, and 4 graminoids) grew on the talus, but only plants showing relevant geomorphic interactions will be mentioned here. Infre-

quently, stems in some plants, such as *Eriogonum* spp. or *Holodiscus microphyllus*, had been scarred and/or crushed by falling rocks. Scrape marks and impact scars (Hétu, 1990) were more common on the trunks of trees, which have invaded a sizable area on the west basal talus (Fig.11). Many trees had wounds on the upslope side of their stems or branches; these were usually 10-50 cm above the ground surface, although some scrapes reached 110 cm height. Most scars were superficial, only bark having been removed, but in some trees several cm of wood had also been eroded; a WW pine on the basal talus (near transect B) had lost bark and wood around 50 % of its girdle from 70 to 210 cm height, and the tree was severely tilted. Another pine on the basal talus (transect D), had an unusual wound: a dacite block (11 x 8 cm) had hit the tree stem and become firmly embedded in it 150 cm above the base (Fig. 12). Most of this damage seems to have been caused by bouncing blocks, but some may also have resulted from snow avalanches (see discussion below).

FIGURE 11.   West basal talus area, directly upslope from Crags Lake. Transect D crosses the photo in the (lower left) foreground. Note the fine particle size prevalent on this segment and the sizable conifers which have colonized the lower talus; the tallest pines on the upper left are ~9 to 13 m tall. The trail to Crags Lake is seen on the right side of the picture. August 1992.

Partie ouest du talus inférieur, directement au-dessus du Crags Lake. Le transect D traverse la photographie au premier plan à gauche. À noter la granulométrie fine qui domine et les grands conifères qui ont colonisé le talus inférieur, les plus grands pins, en haut à gauche, ayant de ~9 à 13 m de hauteur. La piste vers le Crags Lake est à droite (août 1992).

DRY DEBRIS SLIDES

Dry debris slides or 'grain flows' (Lowe, 1976) were a dominant process of debris transport near the talus apex. These mass movements were extremely common in the upper 100-120 m of the talus, which had both a fine debris cover (Table II) and the steepest gradients. Because dry sliding occurs only on slopes at or near the angle of repose (Lowe, 1976; Francou and Hétu, 1989), this was restricted elsewhere to locally steep segments. Debris streaming was infrequent or absent on slopes < 27°, but was repeatedly

FIGURE 12. Upslope side of the trunk of a western white pine growing on the basal talus near transect D. The 25-cm thick trunk has been hit by a bouncing dacite block (11 x 8 cm). Bark has grown around the block, now firmly embedded in the stem at a ~150 cm height. July 1992.

Tronc (face vers le haut) d'un pin blanc croissant sur le talus inférieur près du transect D. Le tronc de 25 cm de diamètre a été heurté par un caillou de dacite (11 x 8 cm). L'écorce , qui s'est formée tout autour, emprisonne maintenant la pierre à ~150 cm de hauteur (juillet 1992).

observed on gravel / pebble areas from ~29° to 34°, which seems to be the steepest gradient reached by fine debris on the Chaos talus. An unusually well-developed sieve effect was found in block areas of the UM and LM zones donwnslope from the finer upper talus (*cf.* Hétu, 1995). Excavation showed only the upper 30 to 50 cm of the block deposits to be 'open-sieve', while small pebbles, cobbles, and gravel uniformly filled all interstices below this depth; this supports the idea that frequent grain flows initiated on the slopes above gradually bring fine sediment to the blockier areas. B. Hétu (pers. comm., 1997) has also observed this process in the Pyrénées.

It should be emphasized that dry sliding was quite pronounced on the steep upper segments of the Crags talus. In some places, extensive sliding occurred *constantly* as I walked across the slope; I believe that, of all the talus slopes I have visited over the past 18 years, the one at Chaos Crags is the most unstable as regards grain flows. The morphology of dry debris slides was similar to that observed elsewhere (Francou and Hétu, 1989; Bertran *et al.*, 1997). Sliding took place along narrow elongated tongues parallel to the slope. Streaming zones had variable size; the smaller events affected strips 1-3 m long, 40-50 cm wide, and a surficial debris layer 10-15 cm thick. The largest debris slides involved zones 12-14 m long, 3-5 m wide, and 20-40 cm thick. Grain flows occurred as a shallow debris layer moved slowly at first, and then accelerated to about 10-12 m min^{-1}; thus, most events were over in < 1 min.

Sliding motion was 'layered', with the upper layer slipping fastest (Matveev, 1963; Hétu *et al.*, 1995). Larger cobbles and blocks remained at the surface while moving quickly over a mass of finer pebbles and gravel; these last actually migrate to, and become concentrated at, the base of the grain flow due to 'kinematic sieving' (Van Steijn *et al.*, 1995). Spherical clasts rolled and bounced swiftly, like marbles. Slab-shaped fragments slid with their *ab* plane parallel to the slope surface, while the *a* axis of elongated particles remained parallel to the slope during descent. Coarser clasts were laterally segregated to form narrow levees, and / or travelled to the base of the sliding mass, where piling up of debris built small bulging lobes (Van Steijn *et al.*, 1995; Bertran *et al.*, 1997). Some larger and more spherical blocks continued rolling beyond the slide to the talus base (Rapp, 1960b) causing small dry 'impact avalanches' (Pérez, 1985) on their way down. Small slip faces often remained at the upslope (detachment) end of grain flows; along with the basal lobes, these produced a characteristic profile of stair-shaped terracettes (Gerber and Scheidegger, 1966). Grain-flow deposits were recognizable as elongated zones with a finer veneer than the surrounding slope (Fig. 13). This is due in part to the quick lateral / frontal segregation of coarser blocks during motion, but also indicates that the surface over which the grain flow stops has already been affected by sieving of fine grains for some time (P. Bertran, pers. comm., 1997).

Presence of isolated blocks also caused a stepped topography, as stable boulders (*blocs freineurs*, Francou, 1986) firmly embedded in the talus obstructed the flow of finer debris, which piled above the rocks. Debris damming generated distinct elongated 'cobble stripes' (Pérez, 1988c) and enormous fine-debris bulges *upslope* from blocks. Lateral deflection of sliding debris toward the boulder edges also created narrow, elongated cobble / pebble tongues extending *downslope* at either side from the blocks (Pérez, 1993). Dislodging of boulders caused sizable slides. While sampling the upper talus near the cliffs, an accidentally loosened, 90 cm-long block began creeping; this destabilized a debris wedge 2.5-3 m wide, 13-14 m long, and 30-50 cm thick, above the block. The debris mass slipped as a unit 6-7 m before stopping, although the largest clasts kept bouncing to the footslope. Elongated debris tongues also formed upslope from plants of all sizes. Small shrubs and compact cushion plants such as prickly phlox (*Leptodactylon pungens*), coyote mint (*Monardella odoratissima*) or phacelia (*Phacelia frigida*) dammed wedge-shaped debris tails 30-70 cm long and 10-20 cm thick. Larger shrubs of rock spirea (*Holodiscus microphyllus*) were often nearly buried by enormous piles of rubble. The trunks of many trees also detained

FIGURE 13. Recent dry-debris slide - from upper left to lower right corners of the photo - on a steep talus (~37°) near the Chaos Crags summit, at 2470 m. A 10 to 15 cm-thick surface layer of cobbles and blocks has been removed by sliding from the elongated tongue, ~3.3 m long and 55 cm wide at the base, now covered by a thin veneer of pebbles and gravel. Photo taken July 23 1989, just minutes after the brief sliding event - lasting only a few seconds - took place.

Coulées sèches récentes sur talus escarpé (~37°) près du sommet des Chaos Crags, à 2470 m. Une couche de 10 à 15 cm d'épaisseur de galets et de blocs a été dégagée tout au long de la langue de glissement (~3,3 m de long sur 55 cm de largeur à la base) maintenant recouverte d'une pellicule de galets et de gravier. La photographie a été prise le 23 juillet 1989, quelques minutes à peine après le glissement qui n'a duré que quelques secondes.

moving debris, and lateral deflection around stems produced clast tongues similar to those near blocks. Like debris, organic litter is also affected by sliding, its overall distribution patterns following those of moving debris; *e.g.*, litter piling produced O horizons 90-170 % thicker upslope from tree stems than downslope (F.L. Pérez, unpubl. data).

Several additional plant characteristics, including their spatial patterns, indicate the severity of dry sliding. Most plants in fine-debris areas grow below boulder dams, as these provide stable shelters against constant talus sliding and burial by moving debris (Pérez, 1994). Rock spirea was particularly common in this type of habitat, where shrub edges sharply coincided with those of boulders, indicating that branches are continuously 'trimmed' by downstreaming debris on both sides of the rock. As a result of this lateral sliding, many small mat-forming plants (*Arenaria kingii*, *Penstemon davidsonii*) growing on unstable talus areas also

attain a clearly downslope-elongated shape, and on one occasion, a line of four small clones - probably part of the same 'individual' - of rock spirea extended 3.5 m below a large boulder shelter.

In addition to these surface features, the roots of most plants indicate that dry grain flows affect them substantially. Excavation of many plant specimens of 30 species common on the taluses of Chaos Crags and other LVNP mountains shows that, invariably, the taproots and buried stems of plants on fine debris areas 'trail' upslope, with 80-100 % of all root biomass located above (Pérez, unpubl. data). This is a common pattern in talus plants (Pérez, 1991a), and is usually ascribed to "...periodic burial by [sliding of] upslope material." (Kershaw and Gardner, 1986: 226). Other root features, such as pronounced layering (formation of new root layers or clusters along buried stems) observed in many specimens of rock spirea and silverleaf lupine also attest to the prevalence of dry sliding on the fine gravelly areas inhabited by these plants.

TRANSPORTATION OF DEBRIS BY SNOW-INDUCED PROCESSES

Because the talus was visited only during summer, no snow avalanches were ever observed, but field evidence indicates that these events play a role in debris transport. Perched blocks (Ward, 1985) were common on the basal east talus, but not on the west end, showing that avalanches occur more frequently below the dacite rockwalls. The greater density of trees on the west side (Fig. 11) would also indicate a lower avalanche frequency there. Several broken tree stumps and severed trunks (2-6 m long and ≤ 35 cm diameter) were found on the footslope; they were missing from the western tip of the site, but became more common in an eastward direction. Tree stumps showed jagged irregular breaks at 30-95 cm height, and were between 21 and 36 cm diameter. This suggests that seedlings and saplings are flexible enough to bend and avoid destruction, but as they grow beyond a critical size they have a greater chance of being killed by snow avalanches. Stumps found were of either WW pine (*Pinus monticola*) or California red fir (*Abies magnifica*). The first may be more frequently destroyed because it is an efficient talus colonizer (most common tree on the slope). Although there were few specimens of red fir, this tree has brittle wood, thus breaks easily and suffers from 'frequent falls' (Munz and Keck, 1970: 50). Many affected trees had survived and produced a dense basal growth by suckering around the severed trunk or layering of surviving branches (Fig.14). Large clonal groups seemed to have produced several generations of upright stems that were broken by successive avalanches.

A fortuitous event illustrates the importance of snow avalanches. During coring in 1992 trees were flagged for identification purposes; in 1993, I could not relocate a WW pine originally on the eastern- and uppermost 'edge of tree colonization' on the talus, 65-70 m above the foot- slope (transect C). A search of the talus revealed a 'new', 70 cm-tall, broken stump with the same diameter (35.5 cm) as the tree cored the previous year. The 8 m-long tree, still bearing

FIGURE 14. Footslope on the east side of the Chaos talus, near transect B. Repeated basal sprouting around a western white pine tree stump, presumably damaged by snow avalanches, has produced a > 4 m diameter clone. Dark arrowhead shows the tip of the broken 90-cm tall, 21-cm diameter, stump. The thin, new upright tree stems are about 185 cm tall. August 1992.

Le pied du versant à la partie ouest du talus des Chaos Crags, près du transect B. La germination répétée autour du tronc d'un pin blanc, probablement endommagé par des avalanches, a produit un clone de > 4 m de diamètre. La flèche montre le bout du tronc de 90 cm de haut et de 21 cm de diamètre. Les nouvelles tiges font à peu près 185 cm de haut (août 1992).

flagging on its branches, was later found on the opposite side of Crags Lake, halfway up the south-facing slope of the 'crater' (Fig. 4D); it had been carried some 125 m from its original location, across the snow-filled depression at the talus base. This pine had an age of ~66 years, and I had previously noted that the tree had a sizable scar on its upslope side and was growing near many broken stumps. This event suggests that: (1) some of the trunk scars noted above (especially larger ones) may be caused by snow avalanches, not by falling rocks; (2) trees have been expanding eastwards along the footslope during the past few decades; (3) under the current snow regime, invading trees may successfully escape avalanche destruction for some time, but eventually their stem flexibility is reduced and they succumb to one large-scale event.

Several trees on the basal talus had accumulated much fine debris - mostly pebbles - on their lower branches, up to ~80 cm height; this was especially noticeable on red fir, which has a close foliage that traps and retains fine debris well. Most trees with pebbles on their branches had dense basal, layered foliage which had grown around stumps (Fig. 14); some layered trees were also buried by fine debris up to ~75 cm height. This sediment was probably deposited by dirty snow avalanches. Alternatively, such deposition may have resulted from debris flows and / or *debris gliding* over snow, both common processes on the talus slopes of Lassen Peak (Pérez, 1988a, 1989, 1990a). Debris could be gradually transferred to tree branches as the snow cover melts; height of deposition on a tree may indicate snow depth at the time of the deposition event. Gliding over snow could also have produced some of the 'perched' blocks noted above

(see discussion below). Hétu (1989, 1990) reported on the multiple roles of snow on talus slopes in Québec, including that of rapid *snow creep*, but the lack of push ridges or other relevant features on the Chaos talus argues against the effectiveness of this and similar snow-induced processes.

DEBRIS- AND MUD-FLOWS, AND ADDITIONAL PROCESSES OF DEBRIS TRANSPORT

Debris flows were never observed in progress, but their dry tracks, levees, and terminal fans were common on fine-debris areas, especially on the upper slope and on the west end of the talus (Fig. 15). Most debris-flow tracks were short (a few meters long) and restricted to gravel / pebble zones near the talus apex; observations on Lassen Peak (Pérez, 1989) indicate that many flows originate below snowbanks by rapid melting during spring, but rainstorms probably cause some as well. Meltwater also produces much *runoff*, even if just for short distances; part of the fine matrix in between talus blocks may have been transported by running water. Many debris flows start in the couloirs along the rock-wall base due to ample snow accumulation and fine-debris availability (Fig. 3). An extensive area on the UM segment of transect C had been affected by sizable debris flows, which had incised the talus with long, narrow (1-2 m) tracks. Channels had been filled later with pebbles/cobbles, forming networks of long 'rock streams' (McSaveney, 1971; Pérez, 1986) coarser than the flanking levees, with a finer gravel / pebble texture. In the Andes (Pérez, 1991b), clasts are heaved from levees by needle ice, then settle mainly in the tracks to form these peculiar rock streams, but clast sorting on the Chaos talus may be primarily gravitational. Cobble streams - especially steeper, longer ones - were very unstable and easily set in motion by dry sliding (*cf.* Matveev, 1963), thus allowing for a quick clast transfer to lower slope areas.

Although most debris-flow activity occurs high on the talus, some large events reach the basal slope. During the 1990-91 season, a huge debris flow originating in a couloir at the cliff base travelled > 400 m to the footslope, where a large terminal fan 30-40 m wide and 1.5-2 m thick was built (Fig. 15). This fan, like the flow tracks, was composed of fine gravel heavily armored with large blocks and cobbles buoyed up by the fluid mass. Many older, eroded tracks are still evident throughout the west talus, indicating that sizable events are not uncommon.

Additional agents of debris movement on the Chaos talus might include disturbance by needle ice and other types of frost. *Needle ice* may cause much debris transport on fine talus (Pérez, 1985, 1993; Francou, 1986) and I have often observed signs of its activity (soil nubbins, striated soil, stone gaps) on the slopes of Lassen Peak (Pérez, 1984, 1989). This field evidence, however, was lacking at the Chaos site. The mean content of fines (< 0.063 mm) for the soils of the Chaos talus is only about 4.2 % (Pérez, unpubl. data) in contrast to ≤ 23 % in the older talus on Lassen Peak (Pérez, 1989). A minimum amount of fines is needed for adequate water migration to the freezing surface, and soils with ≤ 8 % fines do not allow needle ice to form even if saturated

FIGURE 15.   Recent debris-flow deposits on finely-textured talus. The large debris-flow track and terminal fan were produced by events during Spring (?) 1991. The basal fan is about 40 m wide. Several smaller, older, and partially eroded debris-flow tracks appear also on the upper right side of the photograph, taken August 1991 between transects C and D.

Dépôts de glissement récents sur talus à texture fine. La grande trace de glissement et son cône terminal ont été formés au cours du printemps (?) de 1991. La largeur du cône est d'environ 40 m. Plusieurs autres plus petits glissements, plus anciens et partiellement érodés, apparaissent au côté droit supérieur (photographie prise en août 1991, entre les transects C et D).

(Meentemeyer and Zippin, 1981; Pérez, 1984). It must therefore be concluded that the recent soils on the Chaos talus are simply too coarse to produce needle-ice growth.

INTEGRATION OF RESULTS AND OBSERVATIONS

Morphometric data and profiles (Table I, Fig. 4) show all talus sections were bisegmented and had a strong basal concavity (Francou and Manté, 1990). There was a sharp reduction in gradient and a change in slope form from rectilinear to concave near the footslope, but this slope break took place at a lower angle (~20°) than that reported by these authors (33°). This inflection might simply reflect the shape of the underlying surface created during the volcanic explosion. The high concavity attained by transect D could indicate either significant avalanche or debris-flow activity, but as field evidence suggests the first process was not very active there, the concavity may be ascribed to debris flows. The complex micro-topography of old channels, levees, and lobes on this basal talus (Fig. 15) also suggests an important role for debris flows.

There was a noticeable gradient in particle size across the slope, related to the height of cliffs above the talus (*cf.* Pérez, 1989); the larger and more abundant clasts found below rockwalls suggest that present debris supply exerts an important control on talus morphology.

The pronounced within-talus variation in surficial talus texture, clast size and fabric, and the field observations on geomorphic activity indicate a strong stratification of dominant processes of debris transport along the slope. The upper talus, with few and small clasts scattered over fine

gravel, is affected mainly by dry grain flows, which allow particles to creep and slide downhill with their *a* axes roughly parallel to the slope plane and direction (*cf.* Van Steijn *et al.*, 1995), as this alignment offers the least frictional resistance (Statham, 1973). Creeping clasts develop an imbricate arrangement as they stop against other particles on the slope (Albjär *et al.*, 1979). The strong imbrication observed also indicates the significance of dry sliding. In contrast, the large blocks which cover the lower talus are mainly deposited by rockfall. Big stones, while rolling and bouncing, tend to rotate about their long axes, which become aligned with the contours (Caine, 1967) (Fig. 10A-L); but after colliding with other blocks on the talus, this orientation may not be preserved, and most clasts attain an isotropic fabric (Fig. 10B-L). These processes also effect a normal downslope size sorting. The weaker shape sorting found downtalus also conforms with the proposed process stratification. Compact, isometric blocks rotate easily when set in motion and reach the footslope, but platy / elongated particles move chiefly by creep, and friction normally arrests their descent well before they reach the talus base.

The reversed size sorting on upper transect B (Fig. 7B) is unusual, especially since it is under the tallest cliff zone. Clasts falling on this area should readily bounce downtalus *if* they landed on the bare slope. Perhaps rockfalls during winter, when the talus is covered by snow, have affected this zone recently in a manner similar to that described above for the rockfall event in 1990-91. This would allow sizable boulders to remain on the upper talus, but it is not apparent why the nearby transect A, also below tall cliffs, does not display a comparable sorting.

Within-plot sorting on talus is seldom discussed, and seems poorly understood. The low sorting indices found on most plots (Table II) suggest that fragments are efficiently segregated along the slope. This may result from frequent debris transportation, which should generate a better sorting (*cf.* Folk, 1980). In addition to rockfall, dry sliding seems particularly effective in causing sorting by nearly constant debris transfer down the talus. Surficial sorting is greatly affected also by the sieve effect, which gives the external *appearance* of particle homogeneity when in reality debris at depth are much more heterogeneous and unsorted.

Ample field evidence shows that snow avalanches occur on all but the western tip of the talus, where many large trees grow (Fig. 11). Field observations also indicate that debris flows frequently transport significant amounts of rubble on the west half of the slope (Fig. 15). The spatial segregation of debris flows and snow avalanches across the talus produces a 'secondary' gradient, which superimposed on the primary (rockfall / dry slides) trend down the slope generates a complex spatial pattern of geomorphic activity on the Chaos talus (Fig. 16).

Vector magnitude (L %) values on the Chaos slope were somewhat higher than those found on most taluses (Bertran *et al.*, 1997: table 1), especially near the slope apex, where values as high as 44.7 and 45.4 were encountered (Table IV). Bertran *et al.* (1997: 2, 5) noted that on rockfall talus
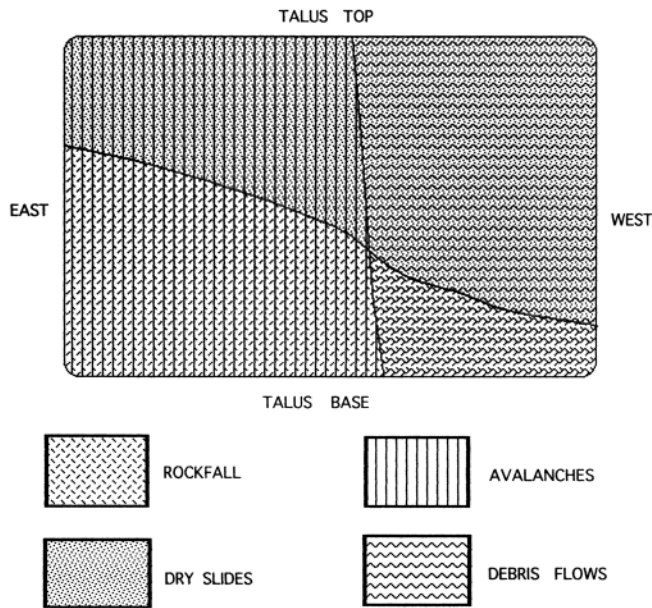
FIGURE 16. Schematic model depicting spatial patterns of dominant geomorphic processes on the Chaos talus. A primary downslope gradient occurs because dry slides are the most significant process of debris transport on the upper talus - particularly on its west side - while the basal talus is mainly affected by rockfall deposition. A secondary gradient across the slope results due to the prevalence of snow avalanches on the east half of the talus below the tall rockwalls, whereas its west section is frequently disturbed by debris flows, especially on the upper slope. Juxtaposition of the gradients causes a complex pattern of process occurrence on each talus area. Transects A and B were on the left side of the graph, C and D on the right one.

Modèle schématique représentant les types de processus géomorphologiques dominants sur le talus des Chaos Crags. Un gradient vertical dominant apparaît en raison des coulée de pierres sèches qui représentent le processus de transport le plus courant dans la partie supérieure du talus, particulièrement dans la partie ouest, tandis que les chutes de pierres atteignent surtout la partie inférieure. Un gradient secondaire résulte de la prédominance des avalanches sur la partie est du talus sous les hauts murs rocheux, alors que les coulées de débris perturbent fréquemment la partie ouest, particulièrement vers le haut. La superposition des gradients produit un modèle complexe de processus qui se produisent dans chacune des parties du talus. Les transects A et B se trouvaient sur la partie gauche du graphique, alors que C et D, sur la partie droite.

"The values of L are low, ...[up to] 27.8%...with a mean of 21.2%..." but also indicated that "...persistent snowbanks may act as a sliding surface for debris falling from the rock wall, causing... L values close to 45%...", and that other talus slopes in mid-latitude mountains where snow lingers are characterized by equally high L % values (Francou, 1983, 1988; Hétu, 1995). This strongly suggests that particle gliding over a hardened snow cover may be a significant factor in debris transport and / or deposition along the Chaos talus.

With few notable exceptions (Kershaw and Gardner, 1986; Hétu, 1989, 1990; Pérez, 1994) talus geomorphologists have made little use of botanical indicators of process activity. This study underlines the potential value of vegetation as an important source of evidence for geomorphic activity and pattern. Tree dating at the Chaos talus suggests

a greater role of snow in the recent past. The largest (76 cm diameter at +30 cm), oldest tree on the basal talus was a WW pine assigned in 1993 a likely age of 134 ± 5 yrs; this tree may have invaded around 1859. Two unrelated events may have triggered tree invasion in the 1850s. Treeline expanded quickly in California during that decade, with a warming trend that began at the end of the Little Ice Age. Subalpine forest expansion on Lassen Peak took place from 1842 to 1880 (Taylor, 1995). Fox-tail pine (*Pinus balfouriana*) invaded timberline in the Sierra Nevada after 1850 (Scuderi, 1987), and regeneration of bristlecone pine (*P. longaeva*) in the White Mountains also occurred after 1850 (LaMarche, 1973). Tree growth occurred because growing-season length at timber-line is controlled by duration of snow cover (Taylor, 1995). Most likely, snow-avalanche frequency also decreased on the Chaos talus after ~1850. A local event may have helped tree colonization of the Crags as well. As noted, the dome adjacent to the talus was "...constantly emitting large quantities of steam and gases..." from 1854 to 1857 (Williams, 1932: 347). The correspondence of these dates with the presumed time of initial pine germination indicates at least the probability that these steam eruptions could also have contributed to a longer snow-free season in the vicinity of the Crags 'crater'.

An initial premise of the study was that the uncommon origin and recency of the Chaos talus might, somehow, make it uniquely different from other, much older taluses. However, the patterns of debris sorting, texture and fabric, as well as geomorphic activity, are similar to those of many talus slopes in the Lassen area. Some reports (Eisbacher, 1979: 318; Bertran, 1996) indicate that sturzstroms normally deposit little or no material on the breakaway surface, which is "...for most of its area...swept clear of debris during the collapse". These studies, coupled with the absence of major distinctive features on the Chaos talus, suggest there is no compelling reason to accept the model of direct debris deposition by the VDAs of 1675, and that most of the talus deposits on the mountain scar were added after the collapse event.

The only striking - if not easily quantifiable - feature of the Chaos talus relates to the extreme instability of most of the slope, and to the inordinately high frequency of dry sliding events observed. Allen (1970: 348) noted that grain flows, although "...the dominant process shaping many screes...", will occur infrequently if sediment supply to the talus remains low, but with large deposition rates from rockwalls, such sliding becomes more continuous and affects larger portions of the talus. Hétu *et al.* (1995) studied a relict talus in the French Pyrénées, where dry grain flows played a significant role in slope evolution, and concluded that frequent, sizable dry sliding events could only have been maintained by constant delivery and renewal of debris supply at the talus apex. This may have resulted from either high rates of rock weathering, or the recurrent agency of some releasing event, probably seismic activity (B. Hétu, pers. comm., 1996). Occurrence of dry grain flows should also have been facilitated by the fact that the brecciated dacites of the Chaos cliffs tend to easily break down in small gravel to pebble-sized fragments (*cf.* Hétu *et al.*, 1995).

The extreme sliding activity observed at the Chaos Crags suggests that either the present rates of (fine) debris supply to the upper slope remain unusually high, or that much of the sediment produced following the genesis event 325 years ago is still resting on the upper talus. Instances of similar rapidly-formed slopes are scarce in the literature. Clark *et al.* (1972) reported on the rapid growth of a talus cone in the Chugach Mountains (Alaska) following the great 1964 earthquake. During a 6-yr period, the weakened, unstable rockwalls supplied ~1.3 million m^3 of debris to a cone about 5 times smaller than the Chaos talus (area estimated from Fig. 1, Clark *et al.*, 1972). Unfortunately, no follow-up studies seem to have been carried out, and it is not known if this talus continued growing at an accelerated pace afterwards. Mills (1992) followed the unusually swift accumulation of several 80-100 m thick talus cones during an 8-yr period after the 1980 eruption of Mount St. Helens, where rockwalls are also andesitic / dacitic. Most cones experienced a peak growth rate during the first 3 years, and although mass-wasting declined subsequently, rates are expected to remain high for some decades. Mills (1992: 745) even suggests that

"...the most intense interval of mass wasting occurred within hours or days of the formation of the crater walls, when the cliffs were most out of equilibrium". The description by Clark *et al.* (1972: 227) of rockfall activity also implies that cliff instability was highest within 2 or 3 years after the earthquake, with only "intermittent rockfalls" occurring by 1970.

The studies above indicate that multiple sizable rockfalls might have occurred in the weakened Crags cliffs following dome collapse, and that they would have swiftly added debris to the talus for some years, until the fractured dacite walls attained at least some precarious stability. In this view, the bulk of the debris on the Chaos talus arrived quickly after the 1675 volcanic explosion, although subsequent events (the steam eruptions of 1854-57, seismic activity) may also have dislodged much debris from the deeply fractured cliffs (Fig. 3). Photo repeat analysis does not disprove this hypothesis, as it indicates the Chaos talus has not changed significantly during the past century. Loomis (1926: 114) took a photograph, which included part of the talus, sometime between 1900 and 1910. (This photograph is not shown due
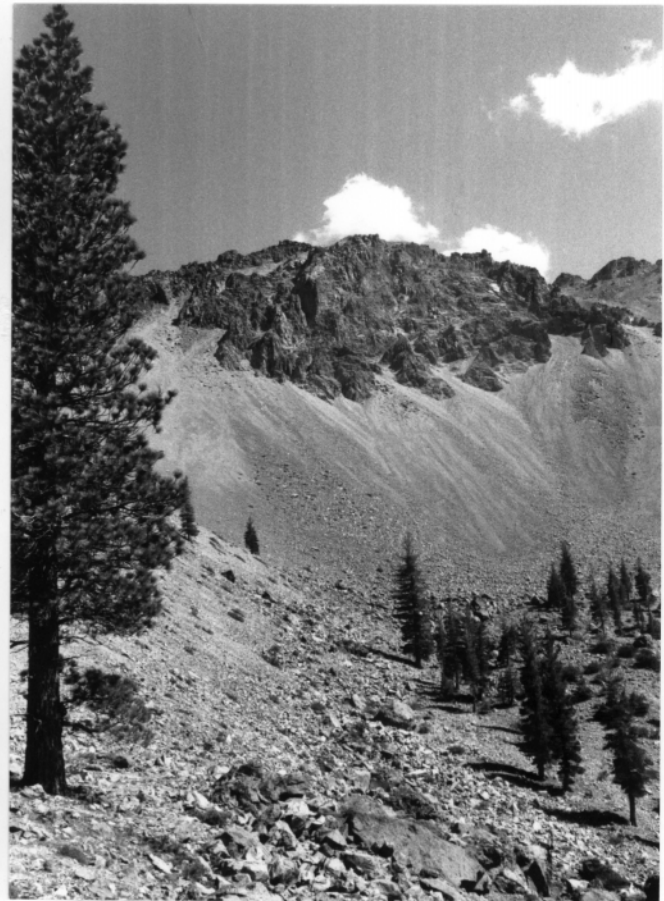

FIGURE 17. Left: Photograph of the east side of the Chaos talus, taken by Williams (1928: Fig. 7) during the summer of 1927 (Williams, 1932: 195). The original figure caption read: "Part of the crater at the northern base of the Chaos Crags." Right: Same talus area in August 1992. Note the overall similarity in the outlines of the dacite walls at their junction with the talus. Vegetation growth is noticeable in the tree group on the lower right of both photographs.

À gauche, photographie de la partie est du talus des Chaos Crags, prise par Williams (1928, fig. 7) au cours de l'été 1927 (Williams, 1932: 195). La légende disait qu'il s'agissait d'une partie du cratère à la base septentrionale des Chaos Crags. À droite, la même partie du talus photographiée en août 1992. À noter la similarité générale de la configuration des murs de dacite à leur rencontre avec le talus. Observer la croissance de la végétation du groupement d'arbres dans le coin inférieur droit.

to its poor, grainy quality). Williams (1928: fig. 7) replicated the view in 1927, but no major differences could be ascertained between shots. Comparison between 1927 and the present (Fig. 17) indicates a similar slope topography and little or no alteration in the outline of the rockwalls along their junction with the talus, but perhaps a slight upslope expansion of the talus areas covered by boulders. Tree cover has increased noticeably along the footslope during the past 70 years, and the density of shrubs (rock spirea) on blocks also appears to be somewhat higher (see Fig. 5).

In summary, the above findings would support the following conclusions:

(1) The lack of major distinctive morphological characteristics on the Chaos Crags talus does not support the hypothesis that debris were instantaneously deposited by VDA events. *If* such was the case, no unusual features created by the volcanic explosion have survived. Instead, the talus attributes examined suggest slope evolution by post-eruptive sedimentation.

(2) Due to the unstable nature of the brecciated rockwalls following dome collapse, the Chaos talus probably accumulated swiftly afterwards. Most debris presumably collected during a short period of a few years. However, without detailed cross-sectional observations of talus deposits (*e.g.*, Hétu, 1995 ; Van Steijn *et al.*, 1995) it is impossible to ascertain whether the nature of the geomorphic processes transporting rubble right after the collapse event was substantially different from that of processes observed today here or on nearby talus slopes.

(3) Some additional, but probably minor, volcanic or seismic events - such as during the period 1854-57 - may well have caused short bursts of debris accretion on the talus.

(4) Slope modification in the recent past and at present occurs by 'normal' mass-wasting processes, although grain flows are particularly active. This appears to be due to an ample supply of fine debris near the talus apex. However, photographs indicate only modest sediment additions and no obvious changes in overall talus morphology during the 20th century.

(5) It seems therefore entirely possible that much of the fine debris resting on the upper talus is part of the 'original' material deposited shortly after dome collapse. In this case, transport processes - though active - have lagged behind the vast initial delivery of debris to the talus.

ACKNOWLEDGEMENTS

REFERENCES

Åkerman, H. J., 1984. Notes on talus morphology and processes in Spitsbergen. Geografiska Annaler, 66A: 267-284.

Albjär, G., Rehn, J. and Strömquist, L., 1979. Notes on talus formation in different climates. Geografiska Annaler, 61A: 179-185.

Allen, J. R. L., 1970. The avalanching of granular solids on dune and similar slopes. Journal of Geology, 78: 326-351.

Arno, S. F. and Hammerly, R. P., 1984. Timberline. Mountain and Arctic Forest Frontiers. The Mountaineers, Seattle, 304 p.

Bertran, P., 1996. Sédimentologie d'une avalanche rocheuse survenue en février 1995 à Claix (Alpes françaises). Quaternaire, 7: 75-83.

Bertran, P., Hétu, B., Texier, J.-P. and Van Steijn, H., 1997. Fabric characteristics of subaerial slope deposits. Sedimentology, 44: 1-16.

Bones, J. G., 1973. Process and sediment size arrangement on high Arctic talus, southwest Devon Island, N.W.T., Canada. Arctic and Alpine Research, 5: 29-40.

Browning, J. M., 1973. Catastrophic rock slide, Mount Huascaran, Peru, May 31, 1970. American Association of Petroleum Geologists Bulletin, 57: 1335-1341.

Brückl, E., Brunner, F. K., Gerber, E. and Scheidegger, A. E., 1974. Morphometrie einer Schutthalde. Mitteilungen Oesterreichische Geographische Gesellschaft, 116: 79-96.

Butler, D. R., Oelfke, J. G. and Oelfke, L. A., 1986. Historic rockfall avalanches, Glacier National Park, Montana, U.S.A. Mountain Research and Development, 6: 261-271.

Caine, T. N., 1967. Texture of talus in Tasmania. Journal of Sedimentary Petrology, 37: 796-803.

_____ 1969a. A model for alpine talus slope development by slush avalanching. Journal of Geology, 77: 92-100.

_____ 1969b. The analysis of surface fabrics on talus by means of ground photography. Arctic and Alpine Research, 1: 127-134.

Carniel, P. and Scheidegger, A. E., 1974. Morphometry of an alpine scree cone. Rivista Italiana di Geofisica, 23: 95-100.

Clark, S. H. B., Foster, H. L. and Bartsch, S. R., 1972. Growth of a talus cone in the western Chugach Mountains, Alaska. Geological Society of America Bulletin, 83: 227-230.

Crandell, D. R., 1972. Glaciation near Lassen Peak, northern California. U.S. Geological Survey, Professional Paper, 800C: 179-188.

Crandell, D. R. and Fahnestock, R. K., 1965. Rockfalls and avalanches from Little Tahoma Peak on Mount Rainier, Washington. U.S. Geological Survey Bulletin, 1221-A: 1-30.

Crandell, D. R., Mullineaux, D. R., Sigafoos, R. S. and Rubin, M., 1974. Chaos Crags eruptions and rockfall-avalanches, Lassen Volcanic National Park, California. U.S. Geological Survey, Journal of Research, 2: 49-59.

Curray, J. R., 1956. The analysis of two-dimensional orientation data. Journal of Geology, 64: 117-131.

David, H. A., 1952. Upper 5 and 1 % points of the maximum F-ratio. Biometrika, 39: 422-424.

Dawson, A. G., Matthews, J. A. and Shakesby, R. A., 1986. A catastrophic landslide (sturzstrom) in Verskildalen, Rondane National Park, southern Norway. Geografiska Annaler, 68A: 77-87.

Doornkamp, J. C. and King, C. A. M., 1971. Numerical Analysis in Geomorphology. St. Martin's, New York, 372 p.

Duncan, D. B., 1955. Multiple range and multiple F tests. Biometrics, 11: 1-42.

Eisbacher, G. H., 1979. Cliff collapse and rock avalanches (sturzstroms) in the Mackenzie Mountains, northwestern Canada. Canadian Geotechnical Journal, 16: 309-334.

Fisher, R. A., 1953. Dispersion on a sphere. Proceedings, Royal Society of London, series A, 217: 295-305.

Folk, R. L., 1980. Petrology of Sedimentary Rocks, 3rd. ed. Hemphills, Austin, 185 p.

Francou, B., 1983. Géodynamique des dépôts de pied de paroi dans l'étage périglaciaire. Revue de Géologie dynamique et de Géographie physique, 24: 411-424.

_____ 1986. Dynamiques périglaciaires et Quaternaire dans les Andes centrales. Rapports scientifiques et techniques, Centre de Géomorphologie, Caen, 2: 1-63.

_____ 1988. L'éboulisation en haute-montagne. Thèse d'état, Centre de Géomorphologie, C. N. R. S., Caen, 696 p + 11 pl.

_____ 1991. Pentes, granulométrie et mobilité des matériaux le long d'un talus d'éboulis en milieu alpin. Permafrost and Periglacial Processes, 2: 175-186.

Francou, B. and Hétu, B., 1989. Éboulis et autres formations de pente hétérométriques. Contribution à une terminologie géomorphologique. Notes et comptes-rendus du groupe de travail "Regionalisation du Périglaciaire", Centre de Géomorphologie, C.N.R.S., Caen, 14: 11-69.

Francou, B. and Manté, C., 1990. Analysis of the segmentation in the profile of alpine talus slopes. Permafrost and Periglacial Processes, 1: 53-60.

Gardiner, V. and Dackombe, R., 1983. Geomorphological Field Manual. Allen & Unwin, London, 254 p.

Gardner, J. S., 1970. Rockfall: A geomorphic process in high mountain terrain. Albertan Geographer, 6: 15-20.

_____ 1972. Morphology and sediment characteristics of mountain debris slopes in the Lake Louise district. Zeitschrift für Geomorphologie, 15: 390-402.

_____ 1983. Rockfall frequency and distribution in the Highwood Pass area, Canadian Rocky Mountains. Zeitschrift für Geomorphologie, 27: 311-324.

Gardner, J. S., Smith, D. J. and Desloges, J. R., 1983. The dynamic geomorphology of the Mt. Rae area: A high mountain region in southwestern Alberta. University of Waterloo, Department of Geography Publications, 19, 237 p.

Gerber, E. K. and Scheidegger, A. E., 1966. Bewegungen in Schuttmantelhängen. Beobachtungen und Versuche einer Theorie. Geographica Helvetica, 21: 20-31.

Goudie, A., 1981. Geomorphological Techniques. Allen & Unwin, London, 395 p.

Griffiths, J. C., 1959. Size and shape of rock fragments in Tuscarora Scree, Fishing Creek, Lamar, central Pennsylvania. Journal of Sedimentary Petrology, 29: 391-401.

Hall, K., 1979. Sorted stripes oriented by wind action: Some observations from Sub-Antarctic Marion Islands. Earth Surface Processes and Landforms, 4, 281-289.

Hartley, H. O., 1950. The maximum F-ratio as a short-cut test for heterogeneity of variance. Biometrika, 37: 308-312.

Heath, J. P., 1959. Dating Chaos Jumbles, an avalanche deposit in Lassen Volcanic National Park. American Journal of Science, 257: 537-538.

_____ 1960. Repeated avalanches at Chaos Jumbles, Lassen Volcanic National Park. American Journal of Science, 258: 744-751.

Hétu, B., 1989. La dynamique des éboulis schisteux au cours de l'hiver, Gaspésie septentrionale, Québec. Géographie physique et Quaternaire, 43: 389-406.

_____ 1990. Évolution récente d'un talus d'éboulis en milieu forestier, Gaspésie, Québec. Géographie physique et Quaternaire, 44: 199-215.

_____ 1995. Le litage des éboulis stratifiés cryonivaux en Gaspésie (Québec, Canada): rôle de la sédimentation nivéo-éolienne et des transits supranivaux. Permafrost and Periglacial Processes, 6: 147-171.

Hétu, B., Van Steijn, H. and Vandelac, P., 1994. Coulées de pierres glacées: un nouveau type de coulées de pierraille sur les talus d'éboulis. Géographie physique et Quaternaire, 48: 3-22.

Hétu, B., Van Steijn, H. and Bertran, P., 1995. Le rôle des coulées de pierres sèches dans la genèse d'un certain type d'éboulis stratifiés. Permafrost and Periglacial Processes, 6: 173-194.

Jones, T. A., 1969. Skewness and kurtosis as criteria of normality in observed frequency distributions. Journal of Sedimentary Petrology, 39: 1622-1627.

Kershaw, L. J. and Gardner, J. S., 1986. Vascular plants of mountain talus slopes, Mt. Rae, Alberta, Canada. Physical Geography, 7: 218-230.

Kirkby, M. J. and Statham, I., 1975. Surface stone movement and scree formation. Journal of Geology, 83: 349-362.

Krumbein, W. C., 1939. Preferred orientation of pebbles in sedimentary deposits. Journal of Geology, 47: 673-706.

_____ 1941. Measurement and geological significance of shape and roundness of sedimentaryparticles. Journal of Sedimentary Petrology, 11: 64-72.

LaMarche, V. C., 1973. Holocene climatic variations inferred from treeline fluctuations in the White Mountains, California. Quaternary Research, 3: 632-660.

Loomis, B. F., 1926. Pictorial History of the Lassen Volcano. California History Books, Anderson, 143 p.

Lowe, D. R., 1976. Grain flow and grain flow deposits. Journal of Sedimentary Petrology, 46: 188-199.

Luckman, B. H., 1976. Rockfalls and rockfall inventory data: Some observations from Surprise Valley, Jasper National Park, Canada. Earth Surface Processes, 1: 287-298.

Major, J., 1977. California climate in relation to vegetation, p. 11-74. In M. G. Barbour, and J. Major, eds., Terrestrial Vegetation of California. Wiley, New York.

Matveev, N. P., 1963. Dynamics and age of talus material and rock streams in the bold mountain zone on the northern Urals (Denezhkin Kamen' Massif). Problems of the North, 7: 233-238.

McSaveney, E. R., 1971. The surficial texture of rockfall talus. M. Sc. Thesis, Ohio State University, 91 p.

Meentemeyer, V. and Zippin, J., 1981. Soil moisture and texture controls of selected parameters of needle ice growth. Earth Surface Processes and Landforms, 6: 113-125.

Mills, H. H., 1992. Post-eruption erosion and deposition in the 1980 crater of Mount St Helens, Washington, determined from digital maps. Earth Surface Processes and Landforms, 17: 739-754.

Munz, P. A. and Keck, D.D., 1970. A California Mountain Flora. University of California Press, Berkeley, 1681 p.

Parker, A. J., 1992. Forest / environment relationships in Lassen Volcanic National Park, California. Journal of Biogeography, 18: 543-552.

Pérez, F. L., 1984. Striated soil in an Andean paramo of Venezuela: Its origin and orientation. Arctic and Alpine Research, 16: 277-289.

_____ 1985. Surficial talus movement in an Andean paramo of Venezuela. Geografiska Annaler, 67A: 221-237.

_____ 1986. Talus texture and particle morphology in a north Andean paramo. Zeitschrift für Geomorphologie, 30: 15-34.

_____ 1987. A method for contouring triangular particle shape diagrams. Journal of Sedimentary Petrology, 57: 763-765.

_____ 1988a. Debris transport over a snow surface: A field experiment. Revue de Géomorphologie dynamique, 37: 81-101.

_____ 1988b. Geocryogenic slope caves in the Southern Cascades. Proceedings, 5th International Conference on Permafrost, Volume 1. Tapir, Trondheim, Norway: 834-839.

_____ 1988c. The movement of debris on a high Andean talus. Zeitschrift für Geomorphologie, 32: 77-99.

_____ 1989. Talus fabric and particle morphology on Lassen Peak, California. Geografiska Annaler, 71A: 43-57.

_____ 1990a. Surficial talus fabric and particle gliding over snow on Lassen Peak, California. Physical Geography, 11: 142-153.

_____ 1990b. Conifer litter and organic matter accumulation at timberline, Lassen Peak. U.S. National Park Service Transactions and Proceedings, 8: 207-224.

_____ 1991a. Soil moisture and the distribution of giant Andean rosettes on talus slopes of a desert paramo. Climate Research, 1: 217-231.

_____ 1991b. Particle sorting due to off-road vehicle traffic in a high Andean paramo. Catena, 18: 239-254.

_____ 1992. Miniature sorted stripes in the Páramo de Piedras Blancas (Venezuelan Andes), p. 125-157. In J. C. Dixon and A. D. Abrahams, eds., Periglacial Geomorphology. Wiley, New York.

_____ 1993. Talus movement in the high equatorial Andes: A synthesis of ten years of data. Permafrost and Periglacial Processes, 4: 199-215.

_____ 1994. Geobotanical influence of talus movement on the distribution of caulescent Andean rosettes. Flora, 189: 353-371.

Porter, S. C. and Orombelli, G., 1980. Catastrophic rockfall of September 12, 1717 on the Italian flank of the Mont Blanc massif. Zeitschrift für Geomorphologie, 24: 200-218.

Rapp, A., 1960a. Recent development of mountain slopes in Kärkevagge and surroundings, north Scandinavia. Geografiska Annaler, 42: 65-200.

_____ 1960b. Talus slopes and mountain walls at Tempelfjorden, Spitsbergen. A geomorphological study of the denudation of slopes in an Arctic Locality. Norsk Polarinstitutt Skrifter, 119: 1-96.

Rapp, A. and Fairbridge, R. W., 1968. Talus fan or cone; scree and cliff debris, p. 1106-1111. In R. W. Fairbridge, ed., Encyclopedia of Geomorphology. Dowden, Hutchinson & Ross, Stroutsburg.

Scheffé, H., 1953. A method for judging all contrasts in the Analysis of Variance. Biometrika, 40: 87-104.

Scuderi, L. A., 1987. Late-Holocene upper timberline variation in the southern Sierra Nevada. Nature, 327: 242-244.

Shreve, R. L., 1966. Sherman landslide, Alaska. Science, 154: 1639-1643.

Siebert, L., 1984. Large volcanic debris avalanches: Characteristics of source areas, deposits, and associated eruptions. Journal of Volcanology and Geothermal Research, 22: 163-197.

Soil Survey Staff, 1994. Keys to Soil Taxonomy, 6th. ed. U.S. Department of Agriculture, Soil Conservation Service, Washington, DC, 524 p.

Statham, I., 1973. Scree slope development under conditions of surface particle movement. Transactions, Institute of British Geographers, 59: 41-53.

Stauffer, M. R., 1966. An empirical-statistical study of three-dimensional fabric diagrams as used in structural analysis. Canadian Journal of Earth Sciences, 3: 473-498.

Steel, R. G. D. and Torrie, J. H., 1960. Principles and Procedures in Statistics. McGraw-Hill, New York, 481 p.

Steinmetz, R., 1962. Analysis of vectorial data. Journal of Sedimentary Petrology, 32: 801-812.

Taylor, A. H., 1990. Tree invasion in meadows of Lassen Volcanic National Park, California. Professional Geographer, 42: 457-470.

_____ 1995. Forest expansion and climate change in the mountain hemlock (Tsuga mertensiana) zone, Lassen Volcanic National Park, California, USA. Arctic and Alpine Research, 27: 207-216.

Thomas, D. A. H., 1973. Multiple comparisons among means. The Statistician, 22: 16-42.

Van Steijn, H., Bertran, P., Francou, B., Hétu, B. and Texier, J.-P., 1995. Models for the genetic and environmental interpretation of stratified slope deposits: A review. Permafrost and Periglacial Processes, 6: 125-146.

Voight, B., Janda, R.J., Glicken, H. and Douglass, P.M., 1983. Nature and mechanisms of the Mount St Helens rockslide-avalanche of 18 May 1990. Géotechnique, 33: 243-273.

Ward, R. G. W., 1985. Geomorphological evidence of avalanche activity in Scotland. Geografiska Annaler, 67A: 247-256.

Watson, R. E., 1956. A test for randomness of directions. Monthly Notices, Royal Astronomy Society, Geophysics Supplement, 7: 160-161.

Williams, H., 1928. A recent volcanic eruption near Lassen Peak, California. University of California Publications in Geology, 17: 241-263.

_____ 1929. The volcanic domes of Lassen Peak and vicinity, California. American Journal of Science, 18: 313-330.

_____ 1932. Geology of the Lassen Volcanic National Park, California. University of California Publications in Geology, 21: 195-385 + 3 maps.

_____ 1941. Calderas and their origin. University of California Publications in Geology, 25: 239-346.